Satellite lines from auto-ionizing states of Fe XVI and the problems with the X-ray Fe XVII lines

G. Del Zanna [1][*] N. R. Badnell[2] and P. J. Storey[3]

[1]*DAMPT, Centre for Mathematical Sciences, University of Cambridge, Wilberforce Road, Cambridge CB3 0WA, UK*
[2]*Department of Physics, University of Strathclyde, Glasgow G4 0NG, UK*
[3]*Department of Physics and Astronomy, University College London, London WC1E 6BT, UK*

ABSTRACT

We present new calculations of atomic data needed to model auto-ionizing states of Fe XVI. We compare the state energies, radiative and excitation data with a sample of results from previous literature. We find a large scatter of results, the most significant ones in the auto-ionization rates, which are very sensitive to the configuration interaction and state mixing. We find relatively good agreement between the auto-ionization rates and the collisional excitation rates calculated with the R-matrix suite of programs and AUTOSTRUCTURE. The largest model, which includes J-resolved states up to $n = 10$, produces ab-initio wavelengths and intensities of the satellite lines which agree well with solar high-resolution spectra of active regions, with few minor wavelength adjustments. We review previous literature, finding many incorrect identifications, most notably those in the NIST data base. We provide several new tentative identifications in the 15–15.7 Å range, and several new ones at shorter wavelengths, where previous lines were unidentified. Compared to the previous CHIANTI model, the present one has an increased flux in the 15–15.7 Å range at 2 MK of a factor of 1.9, resolving the discrepancies found in the analysis of the Marshall Grazing Incidence X-Ray Spectrometer observation. It appears that the satellite lines also resolve the long-standing discrepancy in the intensity of the important Fe XVII 3D line at 15.26 Å.

Key words: atomic data – atomic processes – Sun: X-rays.

1 INTRODUCTION

The Marshall Grazing Incidence X-Ray Spectrometer (MaGIXS) flew in 2021 on a sounding rocket and produced the first ever spectral-imaging data of the solar corona in the X-rays, between about 6 and 30 Å (Savage et al. 2023). The instrument had a wide slit and produced spectroheliograms of an X-ray bright point, which had a temperature of about 2 MK. The strongest emission lines in the spectra were from O VII, O VIII, and the Fe XVII lines between 15 and 17 Å. As discussed by Savage et al. (2023), the modelling of the spectra with the CHIANTI[1] version 10 atomic data (Del Zanna et al. 2021) was satisfactory, except the region between 15 and 15.6 Å, where the predicted model was lower by nearly a factor of 2. This is the important spectral region where the strong Fe XVII resonance and intercombination lines (3C at 15.0 and 3D at 15.26 Å) are present.

Possible calibration problems were excluded, which pointed to a problem in the atomic data. Such a large discrepancy was at first surprising, as R-matrix scattering calculations (cf Hummer et al. 1993; Berrington, Eissner & Norrington 1995) such as those of Loch et al. (2006) and Liang & Badnell (2010) resolved the main long-standing discrepancies between predicted and observed intensities of the strongest Fe XVII lines. Indeed, Del Zanna (2011) showed

excellent agreement, to within 10 per cent, between line intensities calculated with those R-matrix rates and a sample of solar high-resolution observations of active regions and flares. However, two of the weaker lines, the 3D at 15.26 Å and the line at 15.45 Å, were shown by Del Zanna (2011) to be significantly blended in quiescent active region observations, where the plasma has a temperature of about 3 MK.

The discrepancies between theory and observation of the Fe XVII lines, and in particular that of the 3C/3D lines, have been the subject of well over 100 publications, many of which are referenced by Kühn et al. (2022). Such interest in the literature is because Fe XVII provides the strongest lines in the X-rays in laboratory and astrophysical spectra. It is also worth noting that the strong Fe XVII lines can be used to measure the electron temperature, as confirmed for the first time in Del Zanna (2011) (this diagnostic was previously known but the earlier atomic data did not allow such a diagnostic to be used).

It has been known for a long time that satellite lines of Ne-like iron (Fe XVII), i.e. decays to bound states from auto-ionizing (AI) states of Na-like Fe XVI, are present in the 14–18 Å range and blend several Fe XVII lines, although a clear picture of their intensities and wavelengths has not emerged from previous literature, as described below. These satellite lines are expected to be much stronger (relative to Fe XVII) in low-temperature 2 MK plasma. Therefore, they are the likely candidates for the missing flux in the MaGIXS spectra, also considering that the CHIANTI model for these lines was limited.

We present in this paper a selection of results from several new atomic calculations we have carried out and used to calculate the intensities of these satellite lines. The main aim of the paper is to show that indeed the missing flux in the MaGIXS spectra is mainly due to satellite lines from AI states of Na-like Fe XVI. We also note that satellite lines from AI states of Fe XV have also been observed in the same spectral region. We have carried out a preliminary calculation for the satellites from Fe XV but found them much weaker than the Fe XVI lines. The present and further studies are part of a long-term programme within the UK APAP network[2] to provide accurate atomic data for astrophysics and laboratory plasma.

The presence of the Fe XVI satellite lines needs to be carefully taken into account when dealing with the Fe XVII lines for their diagnostic use. Another reason why this work is important is that the satellite lines, once their identification and atomic data are firmly established, could be used for a wide range of unique diagnostic applications for solar active regions but also in general for astrophysical plasma. These include measuring electron temperatures, departures from ionization equilibrium, or non-Maxwellian electron distributions. Satellite lines are usually formed by both inner-shell (IS) excitation and dielectronic capture (DC). Seminal papers are Gabriel (1972) and Gabriel & Paget (1972), while useful reviews are those of Dubau & Volonte (1980) and Del Zanna & Mason (2018). As described in these reviews, in so far as the various diagnostics have only been applied to satellites of He-like ions, hence to very high temperature plasma as in solar flares. Therefore, the Fe XVI satellite lines offer in principle new diagnostic tools to study much lower temperature plasmas, typical of solar active regions.

Section 2 gives a summary of relevant previous studies. Section 3 describes the methods and presents a sample of results with some comparisons with previous calculations. Section 4 gives a sample of comparisons with solar data, while Section 5 gives the conclusions. A full set of atomic data in CHIANTI format is provided online via ZENODO.

2 EARLIER STUDIES

We now give a brief summary of the main studies on Fe XVI AI states which are relevant to this work, in chronological order. Unfortunately, none of the studies we have found in the literature provided a complete set of data (even radiative) that we could use to build a model for comparison with ours. We have also tried to carry out in-depth comparisons with the results in the literature, but very often it has been impossible to identify states. This is not because of the different coupling schemes, but because the very strong mixing within almost all the AI states means that only the energy, parity, and J could be used to try and identify states and transitions. The L, S quantum numbers and even the configuration are often not useful. As some AI states with the same parity and J are very close in energy, the ordering and mixing of states changes considerably from calculation to calculation. It is therefore impossible to even attempt firm comparisons with other calculations when the full set of states is not provided.

Burkhalter et al. (1979) presented laser spectra in the 15.4–16.4 and 16.8–18.0 Å ranges. The spectra had a good resolution, as they were obtained with a 3-m grazing incidence spectrometer. The spectra contained the satellite lines from Fe XVI but also satellite lines from Fe XV and many strong Fe XVII, Fe XVIII transitions. Cowan's multiconfigurational Hartree–Fock code was used to attempt the

identification of several Fe XVI lines from $n = 3$ states. It was clear that satellite lines are blended with many of the strong Fe XVII lines. There were significant discrepancies between the predicted (relative) intensities and the observed ones, as well as between the predicted and observed wavelengths. As the authors pointed out, the identifications were very difficult, partly because all the lines were blended, partly because the procedure was not aided by studies along the sequence (they also analysed similar spectra from Ti). Despite this, several experimental energies appeared in the NIST data base (Kramida et al. 2022) from a reanalysis of the Burkhalter et al. (1979) observations. Details can be found e.g. in Shirai et al. (2000). The NIST experimental energies were included in the CHIANTI v.9 (Dere et al. 2019) model. As we shall see below, several of the NIST experimental energies are clearly incorrect. Inconsistencies in the Burkhalter et al. (1979) identifications were found, although the information was not sufficient to produce a full assessment.

Jupén et al. (1988) revised a previous identification of a single decay among the AI states, observed with the beam-foil method: the $2p^5 3s3p\ ^4D_{7/2}$-$2p^5 3s3d\ ^4F_{9/2}$ transition was identified with a line they observed at 248.36±0.05 Å.

Cornille et al. (1994) provided a limited set of atomic data for the $n = 3$ satellite lines, calculated with the SUPERSTRUCTURE code. Only the total intensity factor F_2 (see below) was provided, along with predicted wavelengths, and a few cross-sections for IS excitation. Some general comparisons with SMM/FCS spectra were provided.

Phillips et al. (1997) used Cowan's code to calculate intensities of the $n = 3, 4, 5$ satellite lines. Although the paper was focused on the Fe XVII lines, the authors provided a table of the strongest $n = 3$ lines formed by DC, also providing a comparison with the Cornille et al. (1994) results. Unfortunately, only a few transitions were listed, and only the total intensity factor F_2 was provided, along with predicted wavelengths. We do attempt to match the states, and provide a comparison with our data below. Some general comparisons with SMM/FCS spectra were also provided.

Bruch et al. (1998) presented radiative data for the $n = 3, 4$ states calculated with Cowan's code and compared them to those calculated earlier by Nilsen (1989) with YODA, a relativistic multiconfigurational Dirac–Fock code. We refer to their tables below when we compare our data with theirs. Unfortunately, the authors only published (total) weighted radiative rates and AI rates.

Brown et al. (2001) provided laboratory evidence that at least three IS satellite lines are present, at 15.12, 15.21, and 15.26 Å. The latter is blending the strong Fe XVII intercombination 3D line. They presented low-resolution X-ray spectra obtained with the Lawrence Livermore National Laboratory (LLNL) electron beam ion trap (EBIT).

Safronova et al. (2002) produced a limited set of radiative data for Na-like ions, calculated with their relativistic many-body codes. Some of the energies are relatively accurate, but the data do not include all the main $n = 3$ configurations or the strongest lines.

May et al. (2005) [M05] presented a series of laser spectra which contained the satellite lines from AI states of Fe XV and Fe XVI and many strong Fe XVII, Fe XVIII transitions. Most spectra had a lower resolution than those of Burkhalter et al. (1979). May et al. (2005) used the Hebrew University Lawrence Livermore Atomic Code (HULLAC) and the Flexible Atomic Code (FAC) to present tables of intensities, wavelengths, and identifications. It is unclear, however, which transitions would be relevant for astrophysical plasma as the laser plasma produces very different spectra.

Aggarwal & Keenan (2007) used GRASP to calculate radiative data for a limited set of $n = 3$ states. The energies were not as accurate as those of previous authors.

Liang, Whiteford & Badnell (2008) used the *R*-matrix suite of codes to calculate IS electron-impact excitation (EIE) rates of Fe^{15+} for a set of $n = 3$ states. They included Auger-plus-radiation damping and showed that earlier studies overestimated the rates. The Liang et al. (2008) EIE and the radiative data, calculated with AUTOSTRUCTURE (AS, see Badnell 2011), were included in CHIANTI version 9 (Dere et al. 2019). As the calculation focused on the scattering calculations, the AS energies were not very accurate. The CHIANTI model was complemented with AI rates calculated with AS, using the same set of configurations and the same scaling parameters for the Thomas–Fermi–Amaldi central potential, for consistency.

Graf et al. (2009) [G09] presented high-resolution (about 0.05 Å FWHM) spectra obtained in the 14.5 and 18 Å range with the LLNL EBIT. The spectra contained the strong Fe XVII and IS satellites from Fe XVI. They used FAC to build an atomic model and used the relative intensities to provide a table of line identifications. No details on the atomic calculations or data were given. They also produced calculated spectra from the Cornille et al. (1994) and Phillips et al. (1997) data in a way that was not described, and concluded that the wavelengths and relative intensities based on those previous studies were completely wrong. However, even the comparisons with the FAC model spectra was not entirely satisfactory and complicated by blending with many transitions.

Díaz et al. (2013) [D13] produced a set of accurate energies for the $n = 3$ states, calculated with the relativistic Multireference Moller–Plesset (MR-MP) perturbation theory. For a selection of transitions, they provided wavelengths and a comparison to those calculated by May et al. (2005) with HULLAC. They also report a table of identifications presumably based on wavelength coincidences with the observations reported by Graf et al. (2009). As Díaz et al. (2013) provided the full set of energies, it was possible to identify the correspondence with our calculations in most cases.

Beiersdorfer, Diaz & Ishikawa (2012) used the Díaz et al. (2013) energies and a set of unpublished FAC calculations to revise several previous identifications of IS satellites suggested by Graf et al. (2009). The authors also attempted to identify IS lines in a *Chandra* spectrum of Capella, although in that spectrum the lower temperature lines are very weak, and lines from ions hotter than Fe XVII are also present.

In a follow-up paper, Beiersdorfer et al. (2014) used the Díaz et al. (2013) energies and a set of unpublished FAC calculations to indicate the predicted wavelengths of the strongest satellites formed by DC, against the *Chandra* spectrum of Capella. In a similar study, more extended FAC calculations (up to $n = 30$) were used by Beiersdorfer, Hell & Lepson (2018) to predict the intensities of $n \geq 4$ lines formed by DC. No details were provided, although a plot in Beiersdorfer et al. (2011) on what is presumably the same calculation shows the various contributions from AI states, from which it appears that nearly all the flux blending the 3C line comes from AI states between $n = 4$ and $n = 9$.

3 METHODS

Considering only DC, the population N_s of the AI state s of the Na-like iron is determined by the balance between the DC (with rate C^{dc}), auto-ionization and radiative decay to all energetically lower levels:

$$N_{Ne-like} N_e C^{dc} = N_s \left(\sum_k A_{sk}^a + \sum_{f<s} A_{sf} \right), \quad (1)$$

where A_{sf} is the transition probability for a decay to a bound state (decay rate for short), A_{sk}^a is the auto-ionization rate, N_e the electron number density, and $N_{Ne-like}$ the ground-state population of the Ne-like iron. The intensity of the satellite line decay from the state s to the bound state f is therefore proportional to

$$I_{sf}^{dc} = N_{Ne-like} N_e C^{dc} \frac{A_{sf}}{\sum_k A_{sk}^a + \sum_{f<s} A_{sf}} \, . \quad (2)$$

By applying the Saha equation for thermodynamic equilibrium we obtain a relation between DC and auto-ionization rates and find that $C^{dc} \propto g_s \sum_k A_{sk}^a$, where g_s is the statistical weight of the AI state. The intensity of the spectral line is therefore proportional to the factor F_2:

$$F_2 = \frac{g_s A_{sf} \sum_k A_{sk}^a}{\sum_k A_{sk}^a + \sum_{f<s} A_{sf}} = g_s A_{sf} Y \quad [s^{-1}], \quad (3)$$

which for strong lines is of the order of 10^{13} s^{-1} or higher. We provide below tables of these factors F_2, for comparison to earlier literature, when available. We also list the ratio Y, which is an indication of how close the state is to LTE: when the AI rate $\sum_k A_{sk}^a$ is much larger than the decay rate, $Y \simeq 1$, and the uncertainty in the AI rate does not have a significant effect on the line intensity.

Clearly, the actual line intensity does not scale linearly with the factors F_2 if the IS excitation is significant. As the Na-like iron does not have metastable states for coronal densities, IS excitation can only be a significant populating process for strong decays to the ground state. Generally, the intensity of the satellite line depends both on DC and IS. Our approach is to obtain the intensities of the satellite lines by solving the collisional-radiative matrix which includes both the Na- and Ne-like ions, using the IDL codes developed by one of us (GDZ) and made available to the community via CHIANTI version 9, as described in the Appendix of the paper. We adopt the total dielectronic recombination (DR) rate coefficients between the ground states of the Ne- and Na-like iron from the UK APAP network. We also include in our model level-resolved radiative recombination, with the data also from the UK APAP network.

We do not attempt to model the high-density laser spectra, for a number of reasons. First, many excited states become populated and CE rates need to be included. Secondly, level-resolved recombination needs to be included in the model. Thirdly, the treatment of the DR process does not include transitions among the AI states (collisional redistribution before they can relax via radiation or auto-ionization), which become non-negligible for high-density plasma. Fourth, continuum lowering also needs to be modelled. Fifth, plasma conditions are such that non-Maxwellian electron distributions and time-dependent effects naturally arise in the plasma. Sixth, modelling the relative abundance of the Ne- and Na-like ions is non-trivial. Lastly, coupling with the background radiation field in the level population modelling should be taken into account.

The radiative data, A_{sf} and A_{sk}^a, have been calculated with AUTOSTRUCTURE. We have run many calculations by increasing the number of configurations, as described below.

AUTOSTRUCTURE has a very large set of parameters and ways to run a calculation, in other words is extremely flexible. We experimented with different potentials. We tried a new development, which includes the same potential and optimization parameters as used by FAC, but it did not improve the results. We also tried semirelaxed orbitals, where groups of configurations each have their own potential scaling parameters; and also the fully relaxed case, where each configuration (initially) uses its own Slater-Type-Orbital potential built from its occupation numbers and, optionally, this can be iterated to self-consistency. The fully relaxed case produced excellent energies

Table 1. The target electron configuration basis and orbital scaling parameters λ_{nl} for the structure run of the $n = 3$ model.

Configurations				
$1s^2\ 2s^2\ 2p^6\ 3l$ (l = s,p,d)	1s	1.39933		
$1s^2\ 2s^2\ 2p^5\ 3l\ 3l'$ (l, l' = s,p,d)	2s	1.15549	3s	1.13314
$1s^2\ 2s\ 2p^6\ 3l\ 3l'$ (l, l' = s,p,d)	2p	1.09545	3p	1.09941
	3d	1.13123		

for the lowest set of $n = 3$ configurations, but diverged by nearly $10\,000$ cm^{-1} for the highest ones. At the end we used a unique set of orbitals with Thomas–Fermi scaling parameters optimized by minimizing an energy functional which included first the terms from the $n = 2, 3$ configurations, and then iteratively those arising from higher shells.

For the calculation of the A^{a}_{sk} rates, we included the six lowest excited states in the Na-like ion. Finally, we found that the use of the kappa-averaged semirelativistic potential improves the results. We also added two-body non-fine-structure interactions (contact spin–spin, two-body Darwin, and orbit–orbit), Breit and QED corrections.

3.1 CE rates

We have complemented each set of radiative data with AUTOSTRUC-TURE Breit–Pauli distorted wave (DW) calculations with the same target. We included excitations from the ground state as well as the first four excited states, although for most astrophysical applications the population of Na-like iron is all in the ground state. The rates from excited states have been included in the models for a simple assessment of how different the relative intensities of the lines are for high-density plasmas.

Collision strengths are calculated at the same set of final scattered energies for all transitions. 'Top-up' for the contribution of high partial waves is done using the same Breit–Pauli methods and subroutines implemented in the R-matrix outer-region code STGF. The collision strengths were extended to high energies by interpolation using the appropriate high-energy limits, while the temperature-dependent effective collisions strength $\Upsilon(i - j)$ (CE rate coefficients) were calculated assuming a Maxwellian electron distribution and linear integration with the final energy of the colliding electron.

3.2 Other rates

When building the collisional-radiative models, we used the R-matrix CE rate coefficients and radiative data of Liang et al. (2008) for the bound states included in their model. For the Ne-like ion, we adopted the CHIANTI version 10 (Del Zanna et al. 2021) model.

4 A SAMPLE OF RESULTS

We have run many AS calculations. We started with the $n = 3$ set shown in Table 1. This set is more complete compared to that of Liang et al. (2008) (shown in Appendix), as it includes the $2s^2\ 2p^5\ 3d^2$ configuration, not present in the earlier calculation, but that produces strong satellite lines via DC. We have also added configurations with double excitations opening the $2s^2$ shell. We kept the $1s^2$ shell closed. The corresponding bound states were included.

We then increased the size by adding the $n = 4, n = 5$, and $n = 6$ orbitals and corresponding set of configurations. The $n = 6$ model has 120 configurations and 3450 fine-structure levels. Table 2 lists the set of configurations and scaling parameters adopted for this $n = 6$ model.

For each run we compared the energies with the experimental ones from NIST and the Díaz et al. (2013) theoretical energies. We also experimented with opening the 1s shell and triple excitations, but the energies did not improve much.

The $n = 6$ model provided theoretical energies very close to Díaz et al. (2013) and was a baseline to try and identify spectral lines using various observations, and to compare with previous identifications when possible. It provided predictions for all the observable lines. With few exceptions, relatively good agreement with observations was found.

However, considering the Beiersdorfer et al. (2011) results, a further calculation was carried out, including all the main configurations up to $n = 10$, to improve the predictions for the series of satellite lines blending the 3C resonance lines. The size of the model is large (288 configurations for 8886 j-resolved states) but still feasible with the CHIANTI programs. Table 3 lists the set of configurations and scaling parameters λ_{nl} adopted for this $n = 10$ model. The λ_{nl} for $n = 7 - 10$ have been kept equal to the $n = 6$ ones, as it is clear that they vary little with n for a given l. It turns out that the ab-initio wavelengths are better than the $n = 6$ model, although for most transitions up to $n = 5$ the resulting intensities are close to those of the $n = 6$ model.

Finally, to have an estimate of the contributions from even higher configurations, we have carried out a configuration-averaged AS calculation including the same set of configurations up to $n = 30$.

4.1 Energies

Table 4 lists the energies of a few $n = 3$ bound states and those of a selection of AI $n = 3$ states. The configuration and LS labelling is from AS but is often not very meaningful. The first column lists the experimental energies which are from NIST, except a few new tentative identifications, while the second column gives the AS values obtained with the $n = 6$ model. The following two columns list the Díaz et al. (2013) and Liang et al. (2008) values. Table A2 in the Appendix lists the energies as obtained with the $n = 10$ model, which

Table 2. The target electron configuration basis and orbital scaling parameters λ_{nl} for the structure and DW runs of the $n = 6$ model.

Configurations											
$1s^2\ 2s^2\ 2p^6\ 3l$ (l = s,p,d)	1s	1.39863									
$1s^2\ 2s^2\ 2p^6\ 4l$ (l = s,p,d,f)	2s	1.15549	3s	1.13323	4s	1.13105	5s	1.12566	6s	1.12792
$1s^2\ 2s^2\ 2p^6\ 5l$ (l = s,p,d,f,g)	2p	1.09540	3p	1.09919	4p	1.09824	5p	1.09322	6p	1.09651
$1s^2\ 2s^2\ 2p^6\ 6l$ (l = s,p,d,f,g,h)	3d	1.13139	4d	1.12449	5d	1.11611	6d	1.11910		
$1s^2\ 2s^2\ 2p^5\ 3l\ nl'$ (l = s,p,d,	4f	1.22747	5f	1.19739	6f	1.20392				
n = 3-6,l' = s,p,d,f,g,h)										
$1s^2\ 2s\ 2p^6\ 3l\ nl'$ (l = s,p,d,	5g	1.33528	6g	1.35001	6h	1.0				
n = 3-6,l' = s,p,d,f,g,h)										

Table 3. The target electron configuration basis and orbital scaling parameters λ_{nl} for the structure and DW runs of the $n = 10$ model.

Configurations											
$1s^2\,2s^2\,2p^6\,3l$ (l = s,p,d)	1s	1.40272									
$1s^2\,2s^2\,2p^6\,4l$ (l = s,p,d,f)	2s	1.14452	3s	1.15069	4s	1.12	5s	1.12052	6s	1.12065
$1s^2\,2s^2\,2p^6\,5l$ (l = s,p,d,f,g)	2p	1.08489	3p	1.08734	4p	1.08916	5p	1.08936	6p	1.08962
$1s^2\,2s^2\,2p^6\,nl$ ($n = 6-10$, l = s,p,d,f,g,h)	3d	1.10032	4d	1.11	5d	1.11005	6d	1.11135		
$1s^2\,2s^2\,2p^5\,3l\,nl'$ (l = s,p,d, n = 3-10,l' = s,p,d,f,g,h)	4f	1.18687	5f	1.18174	6f	1.18411				
$1s^2\,2s\,2p^6\,3l\,nl'$ (l = s,p,d, n = 3-10,l' = s,p,d,f,g,h)	5g	1.31015	6g	1.32363	6h	1.10890				

Table 4. List of the main states.

i	Conf.	P	T	E_{exp}	E_{AS}	$E_{\mathrm{Diaz+}}$	$E_{\mathrm{Liang+}}$
1	$2s^2\,2p^6\,3s$	e	$^2S_{1/2}$	0	0	0	0
2	$2s^2\,2p^6\,3p$	o	$^2P_{1/2}$	277 194	277 711	277 222	276 436
3	$2s^2\,2p^6\,3p$	o	$^2P_{3/2}$	298 143	300 089	298 167	296 534
4	$2s^2\,2p^6\,3d$	e	$^2D_{3/2}$	675 501	676 579	675 463	676 373
5	$2s^2\,2p^6\,3d$	e	$^2D_{5/2}$	678 405	681 330	678 372	679 712
33	$2s^2\,2p^5\,3s^2$	o	$^2P_{3/2}$	5773000?	5 744 641	5 756 556	5 802 584
34	$2s^2\,2p^5\,3s^2$	o	$^2P_{1/2}$	5873000?	5 848 114	5 857 665	5 899 697
35	$2s^2\,2p^5\,3s\,3p$	e	$^4S_{3/2}$	–	5 939 043	5 953 391	5 991 935
36	$2s^2\,2p^5\,3s\,3p$	e	$^4D_{5/2}$	5 982 000	5 967 095	5 980 479	6 020 272
37	$2s^2\,2p^5\,3s\,3p$	e	$^4D_{7/2}$	–	5 973 428	5 986 775	6 026 148
38	$2s^2\,2p^5\,3s\,3p$	e	$^2P_{3/2}$	–	5 974 184	5 987 021	6 027 021
39	$2s^2\,2p^5\,3s\,3p$	e	$^2P_{1/2}$	6 001 000	5 986 456	5 999 543	6 041 011
40	$2s^2\,2p^5\,3s\,3p$	e	$^4P_{5/2}$	6 013 000	5 998 400	6 011 855	6 053 544
41	$2s^2\,2p^5\,3s\,3p$	e	$^2D_{3/2}$	6 013 000	5 999 767	6 012 375	6 053 898
42	$2s^2\,2p^5\,3s\,3p$	e	$^2S_{1/2}$	6042000?	6 016 544	6 027 754	6 076 536
43	$2s^2\,2p^5\,3s\,3p$	e	$^4D_{1/2}$	6 075 000	6 066 510	6 077 192	6 113 566
44	$2s^2\,2p^5\,3s\,3p$	e	$^4P_{1/2}$	6089000?	6 072 233	6 082 835	6 128 206
45	$2s^2\,2p^5\,3s\,3p$	e	$^4D_{3/2}$	6 089 000	6 077 288	6 087 509	6 124 285
46	$2s^2\,2p^5\,3s\,3p$	e	$^2D_{5/2}$	–	6 087 412	6 096 282	6 141 431
47	$2s^2\,2p^5\,3s\,3p$	e	$^4P_{3/2}$	6 096 000	6 089 389	6 100 268	6 138 528
48	$2s^2\,2p^5\,3s\,3p$	e	$^2D_{5/2}$	6 110 000	6 098 693	6 108 077	6 147 237
49	$2s^2\,2p^5\,3s\,3p$	e	$^2D_{3/2}$	6129000?	6 105 380	6 113 831	6 157 761
50	$2s^2\,2p^5\,3s\,3p$	e	$^2P_{1/2}$	–	6 178 837	6 182 346	6 229 457
51	$2s^2\,2p^5\,3s\,3p$	e	$^2D_{3/2}$	6217000?	6 195 854	6 201 702	6 244 142
52	$2s^2\,2p^5\,3s\,3p$	e	$^2S_{1/2}$	6267000?	6 252 510	6 245 187	6 313 279
67	$2s^2\,2p^5\,3s\,3d$	o	$^4P_{5/2}$	6 393 000	6 379 612	6 390 567	6 440 048
73	$2s^2\,2p^5\,3s\,3d$	o	$^4F_{5/2}$	6 406 000	6 394 429	6 404 701	6 453 145
74	$2s^2\,2p^5\,3p^2$	o	$^2P_{3/2}$	–	6 397 961	6 406 003	6 469 670
75	$2s^2\,2p^5\,3s\,3d$	o	$^2D_{3/2}$	6 419 000	6 405 385	6 415 660	6 464 402
76	$2s^2\,2p^5\,3p^2$	o	$^2D_{3/2}$	–	6 413 008	6 422 064	6 455 698
77	$2s^2\,2p^5\,3s\,3d$	o	$^4D_{7/2}$	6 422 000	6 413 123	6 421 329	6 471 649
78	$2s^2\,2p^5\,3s\,3d$	o	$^2P_{1/2}$	6 423 000	6 415 027	6 423 498	6 464 730
79	$2s^2\,2p^5\,3s\,3d$	o	$^2F_{5/2}$	6 425 000	6 415 181	6 423 578	6 476 262
80	$2s^2\,2p^5\,3p^2$	o	$^2D_{5/2}$	–	6 417 371	6 425 339	6 474 699
81	$2s^2\,2p^5\,3s\,3d$	o	$^2P_{3/2}$	6436000 6444100?	6 436 676	6 443 091	6 498 398
82	$2s^2\,2p^5\,3s\,3d$	o	$^4D_{1/2}$	–	6 447 867	6 455 202	6 506 414
83	$2s^2\,2p^5\,3s\,3d$	o	$^4D_{3/2}$	6473000	6 476 481	6 483 365	6 536 053
84	$2s^2\,2p^5\,3s\,3d$	o	$^2F_{7/2}$	6445000	6 480 673	6 485 011	6 546 990
85	$2s^2\,2p^5\,3s\,3d$	o	$^4F_{3/2}$	6 502 000	6 493 786	6 502 061	6 547 383
86	$2s^2\,2p^5\,3s\,3d$	o	$^2D_{5/2}$	6464000	6 495 941	6 501 608	6 549 706
87	$2s^2\,2p^5\,3s\,3d$	o	$^4D_{5/2}$	6 502 000	6 496 993	6 504 077	6 555 370
88	$2s^2\,2p^5\,3p^2$	o	$^2P_{1/2}$	–	6 504 938	6 508 883	6 566 725
89	$2s^2\,2p^5\,3s\,3d$	o	$^2D_{5/2}$	6 516 000	6 508 973	6 514 575	6 569 938
90	$2s^2\,2p^5\,3s\,3d$	o	$^2F_{7/2}$	6 517 000	6 509 407	6 514 871	6 561 652
91	$2s^2\,2p^5\,3p^2$	o	$^2P_{1/2}$	–	6 511 585	6 514 341	6 579 688
92	$2s^2\,2p^5\,3p^2$	o	$^2P_{3/2}$	–	6 528 784	6 531 608	6 592 253
93	$2s^2\,2p^5\,3s\,3d$	o	$^2D_{3/2}$	6530000 6553500?	6 549 199	6 550 184	6 611 638
94	$2s^2\,2p^5\,3s\,3d$	o	$^2P_{1/2}$	6 574 000	6 575 409	6 573 657	6 644 694
95	$2s^2\,2p^5\,3p\,3d$	e	$^4D_{1/2}$	–	6 586 884	6 601 400	6 646 599
96	$2s^2\,2p^5\,3s\,3d$	o	$^2F_{5/2}$	6556000	6 591 507	6 593 543	6 651 977
97	$2s^2\,2p^5\,3p\,3d$	e	$^4D_{3/2}$	–	6 595 119	6 608 991	6 654 887
98	$2s^2\,2p^5\,3p\,3d$	e	$^4D_{5/2}$	–	6 607 993	6 620 899	6 667 902

Table 4 *– continued*

i	Conf.	P	T	E_{exp}	E_{AS}	$E_{\mathrm{Diaz+}}$	$E_{\mathrm{Liang+}}$
99	$2s^2\,2p^5\,3s\,3d$	o	$^2P_{3/2}$	6595000 6620000?	6 617 260	6 616 740	6 686 516
151	$2s^2\,2p^5\,3p\,3d$	e	$^2D_{3/2}$	**6831000?**	6 833 056	6 831 282	6 894 915
152	$2s^2\,2p^5\,3p\,3d$	e	$^2D_{5/2}$	**6837100?**	6 837 436	6 838 045	6 893 483
191	$2s^2\,2p^5\,3d^2$	o	$^2G_{7/2}$	**7135000?**	7 130 233	7 134 361	–
192	$2s^2\,2p^5\,3d^2$	o	$^4F_{5/2}$	–	7 136 863	7 142 053	–
193	$2s\,2p^6\,3s\,3p$	o	$^2P_{3/2}$	–	7 138 849	7 128 949	–
200	$2s^2\,2p^5\,3d^2$	o	$^2F_{5/2}$	**7180800?**	7 183 602	7 186 088	–
201	$2s^2\,2p^5\,3d^2$	o	$^2F_{5/2}$	**7191000?**	7 188 617	7 193 832	–
210	$2s^2\,2p^5\,3d^2$	o	$^2F_{7/2}$	**7236000?**	7 241 831	7 242 818	–
211	$2s^2\,2p^5\,3d^2$	o	$^2D_{5/2}$	**7240000?**	7 251 131	7 246 119	–
212	$2s^2\,2p^5\,3d^2$	o	$^2D_{3/2}$	–	7 257 952	7 253 388	–
213	$2s^2\,2p^5\,3d^2$	o	$^2P_{3/2}$	**7266000?**	7 269 242	7 263 947	–

Note. E_{exp} gives the NIST experimental energies (cm^{-1}), except those in bold which are our tentative values. E_{AS} are our ab-initio AS energies with the $n = 6$ model. $E_{\mathrm{Diaz+}}$ are the energies from Díaz et al. (2013), while $E_{\mathrm{Liang+}}$ are the AS ones from Liang et al. (2008).

illustrates how little the values change with the size of the calculation. A full comparison with the Díaz et al. (2013) energies is provided in the Appendix in Table A3.

Our AS energies are generally very close (within a few thousands of cm^{-1}) to the Díaz et al. (2013) ones, especially for the states producing the strongest solar spectral lines. Note that the uncertainty in the experimental values has a similar magnitude. The comparisons with the experimental energies we have carried out indicate that the Díaz et al. (2013) are the most accurate energies across the literature. This is one of the reasons why we have included them in the table. The other is that the authors provided the full set of states so we could match them against ours with some confidence.

Our energies predict the 2p^{5}3s3p $^4D_{7/2}$ (level No.81) -2p^{5}3s3d $^4F_{9/2}$ (level No.112) transition, identified with a line at 248.36±0.05 Å by Jupén et al. (1988), to be at 245.9 Å, while the Díaz et al. (2013) energies predict 248.5 Å.

Table 4 also clearly shows that the Liang et al. (2008) energies differ by a significant amount, about 40 000 cm^{-1}. This is the reason why the mixing of the states and ultimately the rates obtained with the Liang et al. (2008) model are sometimes quite different than those we have calculated, as shown below.

Table 4 also shows that in several cases the NIST energies must be incorrect, not only because of the large departures from the Díaz et al. (2013) (or our) values, but also because the intensities of their decays do not match solar observations, as briefly outlined below. We have highlighted the main ones, but in several other cases, where a question mark is added, the NIST values might also be wrong.

Unfortunately, we have a circular problem: the published structure calculations provide different wavelengths and intensities, hence different identifications. As pointed out by Burkhalter et al. (1979), studies along the sequence do not help. For a few states producing

Table 5. List of the main transitions from the lowest states formed by DC ($n = 3$ models). F2 values, as well as A_{ji} and AI rates are in 10^{13} s^{-1}.

j	i	C_j	T_j	C_i	T_i	λ Å	F_2 v9	A_{ji} V9	F_2 $n = 3$	Y $n = 3$	A_{ji} $n = 3$	AI v9	AI $n = 3$	R	
33	1	$2p^5\,3s^2$	$^2P_{3/2}$	3s	$^2S_{1/2}$	17.322	0.17	0.064	0.25	0.77	0.082	0.12	0.28	1.10	*
40	3	$2p^5\,3s\,3p$	$^4P_{5/2}$	3p	$^2P_{3/2}$	17.498	0.09	0.031	0.08	0.35	0.037	0.027	0.020	0.53	*
50	3	$2p^5\,3s\,3p$	$^2P_{1/2}$	3p	$^2P_{3/2}$	16.855	0.15	0.075	0.16	0.98	0.083	3.2	4.3	1.31	
51	3	$2p^5\,3s\,3p$	$^2D_{3/2}$	3p	$^2P_{3/2}$	16.895	0.09	0.031	0.09	0.52	0.042	0.12	0.059	1.41	
73	4	$2p^5\,3s\,3d$	$^4F_{5/2}$	3d	$^2D_{3/2}$	17.450	0.11	0.022	0.14	0.61	0.037	0.13	0.068	0.68	*
78	5	$2p^5\,3s\,3d$	$^4D_{7/2}$	3d	$^2D_{5/2}$	17.411	0.16	0.023	0.21	0.72	0.037	0.18	0.098	0.70	*
79	5	$2p^5\,3s\,3d$	$^2F_{5/2}$	3d	$^2D_{5/2}$	17.402	0.14	0.028	0.09	0.56	0.028	0.26	0.068	0.01	*
79	4	$2p^5\,3s\,3d$	$^2F_{5/2}$	3d	$^2D_{3/2}$	17.393	0.12	0.023	0.07	0.56	0.023				
80	4	$2p^5\,3s\,3d$	$^2P_{1/2}$	3d	$^2D_{3/2}$	17.399	0.07	0.039	0.12	0.89	0.069	2.4	1.1	1.70	
80	1	$2p^5\,3s\,3d$	$^2P_{1/2}$	3s	$^2S_{1/2}$	15.569	0.10	0.052	0.11		0.063				
81	5	$2p^5\,3s\,3d$	$^2P_{3/2}$	3d	$^2D_{5/2}$	17.368	0.08	0.038	0.13	0.43	0.078	0.40	0.30	1.86	*
81	1	$2p^5\,3s\,3d$	$^2P_{3/2}$	3s	$^2S_{1/2}$	15.536	0.62	0.28	0.54		0.31				* IS
82	1	$2p^5\,3s\,3d$	$^4D_{1/2}$	3s	$^2S_{1/2}$	15.369	0.62	0.32	0.76	0.95	0.40	10	7.9	1.12	
83	1	$2p^5\,3s\,3d$	$^4D_{3/2}$	3s	$^2S_{1/2}$	15.449	0.40	0.10	0.67	0.97	0.17	8.3	7.9	1.22	
84	5	$2p^5\,3s\,3d$	$^2F_{7/2}$	3d	$^2D_{5/2}$	17.341	0.10	0.013	0.18	0.96	0.023	0.59	0.59	1.15	
85	4	$2p^5\,3s\,3d$	$^4F_{3/2}$	3d	$^2D_{3/2}$	17.163	0.12	0.03	0.20	0.94	0.053	2.2	1.1	1.40	
85	1	$2p^5\,3s\,3d$	$^4F_{3/2}$	3s	$^2S_{1/2}$	15.380	0.11	0.029	0.07		0.019				
88	5	$2p^5\,3s\,3d$	$^2F_{7/2}$	3d	$^2D_{5/2}$	17.127	0.27	0.039	0.32	0.61	0.065	0.24	0.11	0.79	*
90	5	$2p^5\,3s\,3d$	$^2D_{5/2}$	3d	$^2D_{5/2}$	17.130	0.12	0.031	0.13	0.23	0.097	0.099	0.043	0.81	*
90	4	$2p^5\,3s\,3d$	$^2D_{5/2}$	3d	$^2D_{3/2}$	17.122	0.08	0.020	0.06		0.047				
92	4	$2p^5\,3p^2$	$^2P_{3/2}$	3d	$^2D_{3/2}$	16.904	0.07	0.017	0.12	1.0	0.030	34	35	0.84	
92	1	$2p^5\,3p^2$	$^2P_{3/2}$	3s	$^2S_{1/2}$	15.169	0.75	0.019	0.02		0.004				
93	1	$2p^5\,3s\,3d$	$^2D_{3/2}$	3s	$^2S_{1/2}$	15.314	0.64	1.3	4.3	0.69	1.6	0.19	3.6	0.56	* IS
94	1	$2p^5\,3s\,3d$	$^2P_{1/2}$	3s	$^2S_{1/2}$	15.211	1.10	2.5	0.11	0.02	2.6	0.71	0.059	0.04	* IS
96	5	$2p^5\,3s\,3d$	$^2F_{5/2}$	3d	$^2D_{5/2}$	17.014	0.07	0.013	0.19	0.90	0.036	0.33	0.41	0.99	
102	1	$2p^5\,3s\,3d$	$^2P_{3/2}$	3s	$^2S_{1/2}$	15.163	3.6	1.1	3.4	0.84	1.0	5.3	5.6	0.60	* IS

Note. The first columns give the upper j and lower i level number, the main configurations from the CHIANTI v.9 $n = 3$ model and the CHIANTI v.9 wavelength (Å) of the transition. Column 5 gives the F2 value (only the strongest lines with values higher than 5×10^{11} are shown. Note that single observed lines have typical values higher than 10^{13}). The following columns show the CHIANTI v.9 A-values and those with our improved $n = 3$ model, and the total AI rates from the auto-ionizing state. The final column gives R, the ratio between the AI rate as calculated with the same improved $n = 3$ model and with the R-matrix codes.

the strongest lines, we have provided tentative new energies and used them for the comparisons to observations. Details are provided below. We have not attempted to apply semi-empirical corrections to the calculations as implemented within AS, and which would improve the results. They could be applied in the future, once the main transitions will be firmly established with new laboratory and solar spectra.

4.2 Radiative data

Table 5 shows as an example the CHIANTI radiative data, which were obtained from the Liang et al. (2008) $n = 3$ target and those we have calculated with the more extended $n = 3$ sets of configurations and different scaling parameters of Table 1. Only transitions from the lowest AI states and with an intensity factor F_2 larger than 5×10^{11} are shown. Note that typical values of F_2 of observed lines in astrophysical spectra are 10^{13} or higher, although the large number of weak transitions within short-wavelength intervals means that weaker transitions can also be significant. We have removed from the model transitions with branching ratios less than 10^{-5} but the total number of satellite lines, all within 11–18 Å, is over 700 000.

We can see that differences of a factor of 2 in the F_2 values are common, although some transitions, indicated in the last column, are actually mainly formed by IS, and not DC, hence the F_2 value is not related to the actual intensity of the line. Sometimes the differences are related to the decay rate, sometimes with the AI rate.

There are also cases as the first transition in the table where the decay rate is similar but the AI rate is different by nearly a factor of

3. By running many calculations, we found that even small changes in the CI expansion or the scaling parameters can have a large effect on the AI rates, easily by an order of magnitude. On the other hand, the radiative rates are generally less affected. Almost all the AI states are completely mixed, and any small change in the relative energies can have a large effect on the mixing and on the AI rates. The fact that the radiative data are often less affected is due to the different sensitivity to the short- and long-range parts of the wavefunctions.

We are not aware that this important issue has been highlighted in the literature. On the other hand, it is also worth pointing out that a large uncertainty in the AI rate does not affect the line intensity when the ratio Y is close to unity, as the AI state is in LTE (AI rate dominant over the decay rate). We have highlighted in the last column the cases where Y is much lower than 1 and the calculated AI rates vary significantly.

To validate the AS AI rates, we have run a calculation with the $n = 3$ set, switched off the corrections for the two-body non-fine-structure interactions, and run the Breit–Pauli R-matrix (BPRM) suite of codes with a relatively simple Ne-like target (four configurations). We used the Quigley and Berrington method (Quigley & Berrington 1996; Quigley, Berrington & Pelan 1998) to locate resonances and get their widths. This process is time-consuming, so only a sample of values are shown. We are not aware of any such comparison presented in the literature. Table 5 shows the ratio R between the AS AI rates and those calculated from the widths of the resonances.

The comparison with the R-matrix AI rates is reassuring, with typical differences for the stronger transitions of 10–30 per cent. However, in a few cases large differences are present. We have

Table 6. List of the $n = 3$ transitions formed by DC with strongest intensity factor F_2 ($n = 6$ model).

j	i	C_j	T_j	C_i	T_i	λ (Å)	λ(P) (Å)	F_2	Y	F_2(P)	F_2(C)	A_{ji} $n=6$	AI $n=6$	AI $n=3$	AI B98	AI N86	
82	1	2s^2 2p^5 3s 3d	$^4D_{1/2}$	3s	$^2S_{1/2}$	15.509	15.181?	0.72	0.95	1.5?	1.1?	0.38	7.1	7.9	7.9	8.6	
93	1	2s^2 2p^5 3s 3d	$^2D[^2P]_{3/2}$	3s	$^2S_{1/2}$	15.269			3.9	0.67			1.5	3.1	3.6	2.0	5.0	IS
99	1	2s^2 2p^5 3s 3d	$^2P_{3/2}$	3s	$^2S_{1/2}$	15.112	15.148	3.3	0.84	2.4	3.8	0.99	5.5	5.6	3.3	4.2	IS
140	3	2s^2 2p^5 3p 3d	$^4P[^2D]_{5/2}$	3p	$^2P_{3/2}$	15.432		1.1	0.98			0.18	7.4	5.7	5.2	4.5	
143	3	2s^2 2p^5 3p 3d	$^2D_{5/2}$	3p	$^2P_{3/2}$	15.399	15.029?	0.58	0.83	1.1?		0.12	0.58	0.6	4.8e-3	0.013	*
151	2	2s^2 2p^5 3p 3d	$^2D_{3/2}$	3p	$^2P_{1/2}$	15.255	15.221?	7.3	0.88	8.2?	8.1?	2.1	16	13	11	11	
152	3	2s^2 2p^5 3p 3d	$^2D_{5/2}$	3p	$^2P_{3/2}$	15.297	15.138?	4.8	0.85	3.0		0.95	5.3	4.8	3.9	4.2	
153	2	2s^2 2p^5 3p 3d	$^2P_{1/2}$	3p	$^2P_{1/2}$	15.237	15.212	1.7	0.56	1.8	1.7	1.5	2.0	1.9	2.3	2.5	*
154	3	2s^2 2p^5 3p 3d	$^2P_{3/2}$	3p	$^2P_{3/2}$	15.245	15.146?	0.29	0.04	2.8?	2.4?	1.8	0.077	0.025	8e-4	4.8e-3	*
156	3	2s^2 2p^5 3p 3d	$^2P_{1/2}$	3p	$^2P_{3/2}$	15.190		1.5	0.43			1.7	1.3	0.8	2.1	1.8	*
159	3	2s^2 2p^5 3p 3d	$^2P[^2D]_{3/2}$	3p	$^2P_{1/2}$	15.157		1.9	0.91			0.5	5.7	6.0	7.2	5.7	
160	2	2s^2 2p^5 3p 3d	$^2S_{1/2}$	3p	$^2P_{1/2}$	15.066	15.069	1.1	0.76	1.4	1.4	0.7	3.1	2.9	4.2	4.0	*
188	4	2s^2 2p^5 3d^2	$^4G_{5/2}$	3d	$^2D_{3/2}$	15.525	15.496?	1.8	0.97	1.4	1.4	0.31	14	14	16	14	
188	5	2s^2 2p^5 3d^2	$^4G_{5/2}$	3d	$^2D_{5/2}$	15.536	15.464?	0.53		1.1		0.09					
191	5	2s^2 2p^5 3d^2	$^2G_{7/2}$	3d	$^2D_{5/2}$	15.507	15.474	2.1	0.97	2.2	1.7	0.27	8.0	7.7	9.2	8.5	
192	5	2s^2 2p^5 3d^2	$^4F_{5/2}$	3d	$^2D_{5/2}$	15.491		1.0	0.67			0.25	0.8	1.0	1.2	1.3	
193	1	2s 2p^6 3s 3p	$^2P_{3/2}$	3s	$^2S_{1/2}$	14.008		1.2	0.95			0.31	6.7	6.0	7.2	8.2	
196	4	2s^2 2p^5 3d^2	$^4D_{1/2}$	3d	$^2D_{3/2}$	15.424	15.407	0.90	0.63	1.1		0.7	1.2	0.73	1.5	1.1	*
198	5	2s^2 2p^5 3d^2	$^2P[^4S]_{3/2}$	3d	$^2D_{5/2}$	15.385	15.376	0.85	0.82	1.0		0.26	1.2	0.67	1.4	0.9	*
199	5	2s^2 2p^5 3d^2	$^2F_{7/2}$	3d	$^2D_{5/2}$	15.382	15.353	1.8	0.93	2.1	2.0	0.24	3.4	4.2	4.5	5.2	
200	4	2s^2 2p^5 3d^2	$^2F[^2D]_{5/2}$	3d	$^2D_{3/2}$	15.368	15.329	2.8	0.88	7.9	8.8	0.5	5.1	3.7	6.3	2.7	*
200	5	2s^2 2p^5 3d^2	$^2F_{5/2}$	3d	$^2D_{5/2}$	15.379		1.1				0.2	5.1				
201	4	2s^2 2p^5 3d^2	$^2F_{5/2}$	3d	$^2D_{3/2}$	15.356		5.5	0.97			0.9	32	34	6.4	39	
209	4	2s^2 2p^5 3d^2	$^2P_{1/2}$	3d	$^2D_{3/2}$	15.240	15.227	1.4	0.52	1.7	2.0	1.3	1.5	1.6	1.3		*
210	5	2s^2 2p^5 3d^2	$^2F_{7/2}$	3d	$^2D_{5/2}$	15.243	15.205	10	0.96	11	11	1.3	35	36	42	39	
211	5	2s^2 2p^5 3d^2	$^2D_{5/2}$	3d	$^2D_{5/2}$	15.221	15.194	2.8	0.19	3.8	3.3	2.5	0.59	0.61	0.66	0.62	
212	4	2s^2 2p^5 3d^2	$^2D_{3/2}$	3d	$^2D_{3/2}$	15.194	15.170	0.48	0.06	1.7	1.2	1.9	0.18	0.22	0.34	0.43	*
212	5	2s^2 2p^5 3d^2	$^2D_{3/2}$	3d	$^2D_{5/2}$	15.205	15.178	0.18		1.2		0.7					*
213	4	2s^2 2p^5 3d^2	$^2P_{3/2}$	3d	$^2D_{3/2}$	15.168	15.150	1.9	0.62	3.6	2.9	0.76	3.7	3.0	4.3	3.5	
213	5	2s^2 2p^5 3d^2	$^2P_{3/2}$	3d	$^2D_{5/2}$	15.179	15.158	3.7		3.4	4.1	1.5					
214	4	2s^2 2p^5 3d^2	$^2P_{1/2}$	3d	$^2D_{3/2}$	15.077	15.097	1.0	0.81	1.5	1.2	0.59	2.6	2.2	3.3	2.6	

Note. The first columns give the upper j and lower i level number, and the main configurations from the $n = 6$ model. For the lower C_i the $2s^2\,2p^6$ is omitted. The following two columns list the theoretical wavelengths (Å) from the $n = 6$ model and from Phillips et al. (1997) (P). The following three columns list the F2 values from the present $n = 6$ model, the Phillips et al. and Cornille et al. (1994) (C) ones, in units of 10^{13}. Only the strongest observable lines with F2 values larger than 10^{13} are shown. The following columns show the A-values and the total AI rates from the auto-ionizing state, also in units of 10^{13}. The AI $n = 3$ is obtained with the $n = 3$ set and KUTOO = 1. The B98 are the AI rates calculated with Cowan's code by Bruch et al. (1998), while the N86 are the YODA ones from Nilsen (1989). An asterisk in the last column indicates differences in the AI rates that can affect the line intensity, as the ratio Y differs from unity, with the exception of the transitions where inner-shell (IS in the last column) is a dominant process.

verified that they occur when two states that are mixing are very close in energy. Generally, the R-matrix energies are quite different from the AS values, even using the same target, so the mixing of states is often quite different.

Table 6 lists all the main $n = 3$ transitions formed by DC, having an intensity factor F_2 larger than 10^{13}. The results are from the $n = 6$ model. We compare our ab-initio wavelengths and F_2 values with those from Phillips et al. (1997), finding in some cases significant differences. We also compare our F_2 values with those from Cornille et al. (1994), finding a large scatter of values. We list a question mark when the level matching is unclear. We believe that the main differences in the F_2 values are due to the different AI rates used for the three calculations. We list in the last columns the AI rates from two of our calculations, and those calculated with Cowan's code by Bruch et al. (1998) and with YODA by Nilsen (1989). We see large discrepancies even for strong transitions. The most important cases, highlighted with an asterisk in the last column, are when the ratio Y is far from unity. However, with a few exceptions, the scatter of values is within 30 per cent.

4.3 CE rates – DW versus *R*-matrix

One important issue is whether the DW approach provides accurate CE rates, compared to those obtained with the R-matrix codes. As the effect of the resonances is small for the AI states, also considering

the resonances is small for the AI states, one would expect that the DW rates are accurate enough even for the $n = 3$ states.

We found that variations of the order of 20–30 per cent in the CE rates calculated with different targets are common, but are mostly related to the variations in the oscillator strengths of each set of calculations, as one would expect.

We have compared the DW cross-sections and rate coefficients for key transitions formed by IS excitation with those calculated by Liang et al. (2008) using the R-matrix codes and radiation damping, finding overall very good agreement. Fig. 1 shows a comparison of rate coefficients for the strongest transitions, calculated with the $n = 6$ model. The minor differences are related to the different gf values, which are listed in the plot.

5 COMPARISON WITH SOLAR OBSERVATIONS

Clearly, in any laboratory or astrophysical spectra, the satellite lines will always be blended with lines from the Ne-like iron and other ions. As the Na-like abundance peaks around 2 MK in ionization equilibrium, the best spectra would be those of 2 MK plasma. Unfortunately, except for the very low-resolution ones of MaGIXS, no solar spectra of 2 MK plasma around 15 Å exist.

Most of the spectra in this spectral region are of flares or active regions where the peak temperature is at least 3 MK. *Chandra* spectra of cool stars exist but do not have resolution and signal-to-noise comparable to solar spectra.
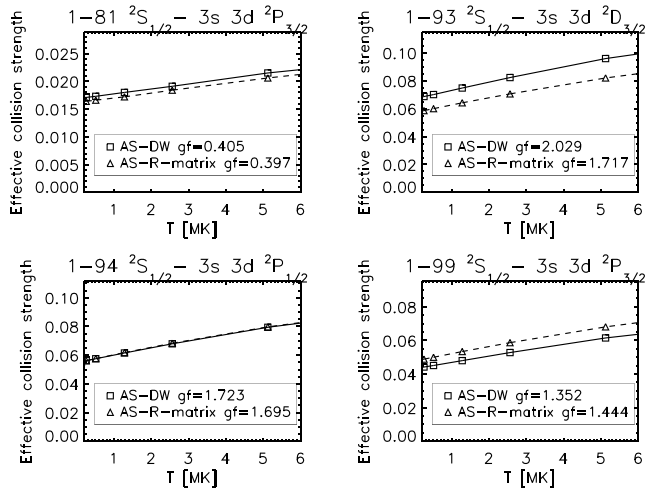
Figure 1. A comparison between the rate coefficients calculated with the DW approximation ($n = 6$ model) and those with the *R*-matrix codes and the $n = 3$ model calculated by Liang et al. 2008
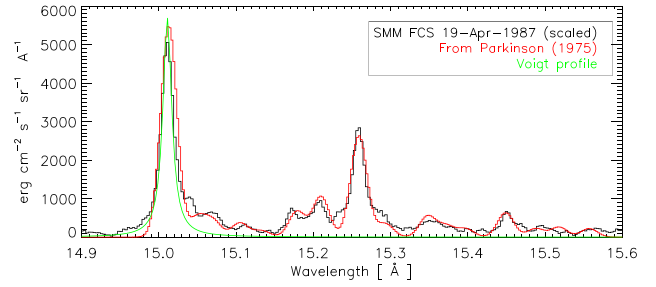

Figure 2. A comparison between the averaged SMM/FCS spectrum of an active region and that reconstructed from the fluxes tabulated by P75, in the spectral region where the main Fe XVII satellite lines are present. The FCS instrumental Voigt profile of the Fe XVII resonance line is shown in green.

The best astrophysical spectrum of the 15–17 Å range, with the Fe XVII lines and their satellites, was taken by a Skylark sounding rocket on 1971 November 30, with Bragg crystal spectrometers built by the University of Leicester (UK) under the supervision of Ken Pounds, pioneer of X-ray astronomy. The spectrum was of a quiescent active region and is high-resolution as the instrumental FWHM was about 0.025 Å. Weak lines were measured, and the wavelength and radiometric calibration was excellent. Details and a table of wavelengths and fluxes are found in Parkinson (1975, hereafter P75). Some results from analyses of this spectrum were published by Del Zanna (2011) and Del Zanna & Mason (2014), where the P75 fluxes were converted to radiances.

The P75 spectra in the plots of the paper appear noisy, and do not clearly show all the measured line intensities listed in the published Table. On the other hand, there are weak features in the spectra that are not listed in the table. To help the atomic data benchmarking procedure, we have created a reconstructed P75 spectrum from the list of the fluxes observed with the KAP crystal, assuming a simple Gaussian broadening with a FWHM = 0.025 Å.

The P75 wavelengths are so accurate, down to a few mÅ, that they have been used as reference wavelengths for several X-ray lines. Most of the weaker P75 lines were unidentified. Several turn out to be due to satellite lines from Fe XVI, as discussed below.

It is interesting to note that the poorly cited laboratory study by Cohen & Feldman (1970) lists several lines which are within a few mÅ of the P75 ones. The spectrum was obtained with a 3m high-resolution spectrograph, from a low-inductance iron vacuum spark. At the time most of the lines were unidentified, but the class of the line listed by Cohen & Feldman (1970) and the wavelength coincidences with the P75 suggests that several of the satellite lines discussed below were also observed in the vacuum spark.

The Solar Maximum Mission (SMM) Flat Crystal Spectrometer (FCS) also produced spectra of quiescent active regions, but with too short exposures and low signal. The instrument was always pointed at the brightest parts, where the hot core loops typically have 3–4 MK. We have searched the entire SMM FCS data base for suitable observations of the satellite lines, but encountered the following problems. First, the count rates of a single bin of each crystal scan are very low, hence to increase the signal to noise several scans need to be averaged. Secondly, significant variability in the strong lines

is often present. In our previous analysis of FCS data (Del Zanna & Mason 2014), we focused on very stable and quiescent scans, where variability is reduced. However, the signal in the satellite lines is too low in those spectra.

We have also analysed spectra during, or after, large flares. In those cases the signal in the lines is generally higher, but that in the satellite lines is lower. Additionally, hotter lines from e.g. Fe XVIII and Fe XIX appear and further complicate the analysis of the spectra.

We found that the best case is a series of five scans taken on 1987 April 19 between 15:54 and 16:42 UT. Some variability was present, and three spectra were scaled by small amounts (10, 20, and 30 per cent) before averaging, to compensate for the variability. The spectrum was then smoothed, converted to calibrated units, and increased by a factor of 2.7 to match approximately the reconstructed AR spectra of P75. The two spectra, plotted in Fig. 2, show a remarkable similarity. The P75 spectrum was clearly of much higher quality, as even the weakest satellite lines were measurable (with about 50 total counts).

The main difference between the observed and reconstructed P75 spectra are the broad features surrounding the Fe XVII 15.01 and 15.26 Å 3C and 3D lines. The FCS instrumental line profile is well approximated with a Voigt function. We have taken the profile of the Fe XVII 16.75 Å line and fitted with a Voigt profile, which is also plotted (rescaled by the peak intensity) in Fig. 2, to show that in fact there is significant signal in the wings of the resonance line at 15.01 Å, especially in the red wing, with two broad features at 15.04 and 15.07 Å, which were listed at 15.05 and 15.07 Å by P75. The main difference is that the broad feature at 15.04 Å is much stronger than the other one, in the FCS spectra. This results from the slightly better spectral resolution of the FCS instrument.

Something similar is present in the red wing of the 15.26 Å line, where P75 list a feature at 15.293 Å, although the FCS spectrum indicates a broader and brighter feature. The FCS spectrum also shows a broad feature in the blue wing of the 3D 15.26 Å line. Inspection of the spectra in Fig. 1(b) of P75 also indicates broadenings around the two Fe XVII lines.

We have slightly improved the previous emission measure analyses of the P75 data described in Del Zanna (2011) and Del Zanna & Mason (2014), and calculated a predicted spectrum. We used CHIANTI v.10 (Del Zanna et al. 2021) data, except for the satellite lines. Table 7 lists a selection of the strongest lines within the P75 spectral range. We list our ab-initio AS wavelength, and the wavelengths of the lines we identify in the Parkinson (1975) and Cohen & Feldman (1970) spectra. Whenever possible, we are also listing the observed wavelengths from Graf et al. (2009). In the last columns we provide

Table 7. List of the strongest satellite lines from AI states of Fe XVI.

Present	B79	P75	CF70	G09	Transition (lower-upper)	I_o	I_p	levels
12.42	–	12.414	12.411?	–	3s ^{2}S$_{1/2}$ - 2s^2 2p^5 3s 4d ^{2}P$_{1/2}$	3.4	-,1.5,1.7,1.6,1.7	1–(336)380
12.42	–	12.414	12.411?	–	3s ^{2}S$_{1/2}$ - 2s^2 2p^5 3s 4d ^{2}P$_{3/2}$		-,1.2,?,2.7,2.8	1–(334)378
12.43	–	-	12.427?	–	3p ^{2}P$_{3/2}$ - 2s^2 2p^5 3p 4d ^{2}D$_{5/2}$		-,2.4,1.6,1.5,1.5	3–(522)566
12.56	–	12.560	–	-	3s ^{2}S$_{1/2}$ - 2s^2 2p^5 3s 4d ^{4}D$_{3/2}$	4.7	-,3.0,2.7,2.5, 2.5	1–(298)342
14.00	–	14.037	14.020?	14.03?	3s ^{2}S$_{1/2}$ - 2s 2p^6 3s 3p ^{2}P$_{3/2}$	4.5	-,0.8,1.3,1.2,1.3	1–(193)237
15.11	15.163p	15.105	15.110	15.111	3s ^{2}S$_{1/2}$ - 2s^2 2p^5 3s 3d ^{2}P$_{3/2}$	9.8	7.2,7.4,6.6,6.7,6.5	1–(99)143
15.17	–	?	15.158?	–	3d ^{2}D$_{3/2}$ - 2s^2 2p^5 3d^2^{2}P$_{3/2}$		-,2.2,1.7,1.6,1.5	4–(213)257
15.18	–	15.179	15.173?	–	3d ^{2}D$_{5/2}$ - 2s^2 2p^5 3d^2^{2}P$_{3/2}$	18	-,4.1,3.1,3.2,3.0	5–(213)257
15.18	–	15.179	–	-	3p ^{2}P$_{3/2}$ - 2s^2 2p^5 3p 3d ^{2}P$_{1/2}$		3.0,2.5,2.4,2.1,2.0	3–(156)200
15.21	15.211p	15.210	15.222?	15.210	3s ^{2}S$_{1/2}$ - 2s^2 2p^5 3s 3d ^{2}P$_{1/2}$	28	18,20.9,21.7,21,21	1–(94)138
15.24	–	15.259(bl 3D)	–	-	3d ^{2}D$_{5/2}$ - 2s^2 2p^5 3d^2^{2}D$_{5/2}$		-,3.4,2.4,2.6,2.4	5–(211)255
15.25	–	15.259(bl 3D)	15.237?	–	3d ^{2}D$_{5/2}$ - 2s^2 2p^5 3d^2^{2}F$_{7/2}$	70	-,12.0,8.9,8.9,8.5	5–(210)254
15.26	–	15.259(bl 3D)	15.261		3p ^{2}P$_{1/2}$ - 2s^2 2p^5 3p 3d ^{2}D$_{3/2}$		8.0,10.6,7.8,7.8,7.3	2–(151)195
15.26	15.314p	15.259(bl 3D)	15.261	15.261	3s ^{2}S$_{1/2}$ - 2s^2 2p^5 3s 3d ^{2}D$_{3/2}$		20,13.8,11.9,13.7,13	1–(93)137
15.29	–	15.293(bl)	15.288?	–	3p ^{2}P$_{3/2}$ - 2s^2 2p^5 3p 3d ^{2}D$_{5/2}$	9.3	4.8,6.9,5.0,5.2,4.9	3–(152)196
15.35	–	15.348	15.341	–	3d ^{2}D$_{3/2}$ - 2s^2 2p^5 3d^2^{2}F$_{5/2}$	14	-,3.6,2.7, 4.4, 4.2	4–(201)245
15.37	–	15.348	15.341	–	3d ^{2}D$_{3/2}$ - 2s^2 2p^5 3d^2^{2}F$_{5/2}$		-,5.8,4.3,3.0,2.8	4–(200)244
15.49	–	15.488	15.490?	–	3d ^{2}D$_{5/2}$ - 2s^2 2p^5 3d^2^{2}G$_{7/2}$	5.9	-,1.9,2.4,2.0,1.9	5–(191)235
15.52	15.538p	15.518	–	15.516	3s ^{2}S$_{1/2}$ - 2s^2 2p^5 3s 3d ^{2}P$_{3/2}$	6.9	3.1,5.3,5.3,3.3,3.3	1–(81)125

Note. The first column gives the present wavelengths (Å). The following three columns indicate the possible wavelength matches from Burkhalter et al. (1979) [B79, p for predicted] and from the lists of the unidentified lines in Parkinson (1975) [P75] and Cohen & Feldman (1970) [CF70]. The next column lists the observed wavelengths from Graf et al. (2009) [G09]. I_o indicates the radiance in erg cm^{-2} sr^{-1} s^{-1} from P75, as described in Del Zanna (2011), while I_p list the predicted values (the first from the CHIANTI model, then those obtained from the $n = 4, 5, 6, 10$ models. The last column indicates the indices of the transition, relative to the $n = 6$ (in brackets) and $n = 10$ models.

the radiances, as measured by P75 and as calculated with the various models.

Clearly, all the satellite lines are blended to some degree, so the comparisons with the spectra, shown in Fig. 3, are more instructive. We have adjusted the energies of a few main states (cf. the energy table) to produce the spectra.

The top plot in Fig. 3 clearly indicates that the CHIANTI (NIST) wavelengths of the main lines are incorrect, with one exception; and that, even for the active region spectra, there is significant missing flux due to the satellite lines. The new $n = 10$ model increases the flux significantly, and brings the predicted intensity of the 3D line in good agreement with observations.

Fig. A1 in the Appendix shows the results from the $n = 6$ model, to show the effects of the additional $n = 7 - 10$ configurations in blending the 3C resonance line.

We have calculated the total flux of the Fe XVII and the satellite lines in the 15–15.7 Å range at 2 MK and found an increase of a factor of 1.93 with the $n = 10$ model (a factor of 1.8 with the $n = 6$ one), relative to the total flux of the current CHIANTI model. Indeed, at such low temperatures, the satellite lines dominate this spectral range.

We discuss below a few details about the main lines, noting that it is nearly impossible to list all previous identifications, whether correct or incorrect. The labelling is from the $n = 6$ model. We are relatively confident about our identifications, but ultimately new high-resolution laboratory and solar spectra will be needed to confirm this work.

5.1 The 15–16 Å region

The strongest line is the decay to the ground state of the 3s3d ^{2}P$_{1/2}$ (level No. 94), mainly formed by IS excitation. The energy of the upper state was estimated by B76 from the decay to the 3d ^{2}D$_{5/2}$, observed at 16.952 Å. The AS ab-initio wavelength is very close (15.21) to the value estimated by B76 (15.211) and to the solar and lab measurements by P75 and G09 (15.210). The predicted radiance is 22, close to the observed one (28.1).

The second strongest line is the decay to the ground state of the 2s^2 2p^5 3s 3d ^{2}D$_{3/2}$ (level No 93), also formed by IS excitation. The B76 predicted wavelength is 15.314 Å, from an energy of 6530 000., obtained from the decay to the 3d ^{2}D$_{5/2}$ at 17.087 Å. This identification is clearly incorrect for various reasons. First, there is no solar line at 15.314 Å. Secondly, the predicted energy is very far from our ab-initio value. Given the predicted intensity and wavelength, this line must be blending the strong Fe XVII 3D observed by P75 at 15.259 Å. The same conclusion was obtained by G09, and earlier by Brown et al. (2001).

Our model predicts a nearby strong line (2–151). We assume it is also blended with the Fe XVII 3D line, which provides an excellent comparison between predicted and observed spectra. With this identification, we obtain an energy of 683 0703 cm^{-1}, close to the value of a state with the same J value and parity given by D13 at 6831 282 cm^{-1}. This line is not listed by G09. What seems to be the same transition (Na5) was predicted by M05 to be at a very similar wavelength, 15.255 Å, but was actually identified with a line at 15.276 Å. As there is no strong solar line at 15.276 Å, the M05 identification seems incorrect.

The third strongest line, mostly formed by IS excitation, is the decay to the ground state from the 2p^5 3s 3d ^{2}P$_{3/2}$ (level No 99), with an AS predicted wavelength of 15.11 Å. The energy of the upper state was estimated by B76 to be 6595 000 from the decay to the 3d ^{2}D$_{3/2}$, observed at 16.890 Å. This predicts the decay to the ground state at 15.163 Å, which is not observed. Again, this was an incorrect identification by B76. We identify, on the basis of wavelength and intensity, with the P75 solar line at 15.105 Å, observed in the laboratory by CF70 and G09 at 15.11 Å.

There are several other cases where the B76/NIST identifications are incorrect. One clear case, where lines are not too blended, is the decay from the 3s 3d ^{2}P$_{3/2}$ (level No. 81). The AS predicted
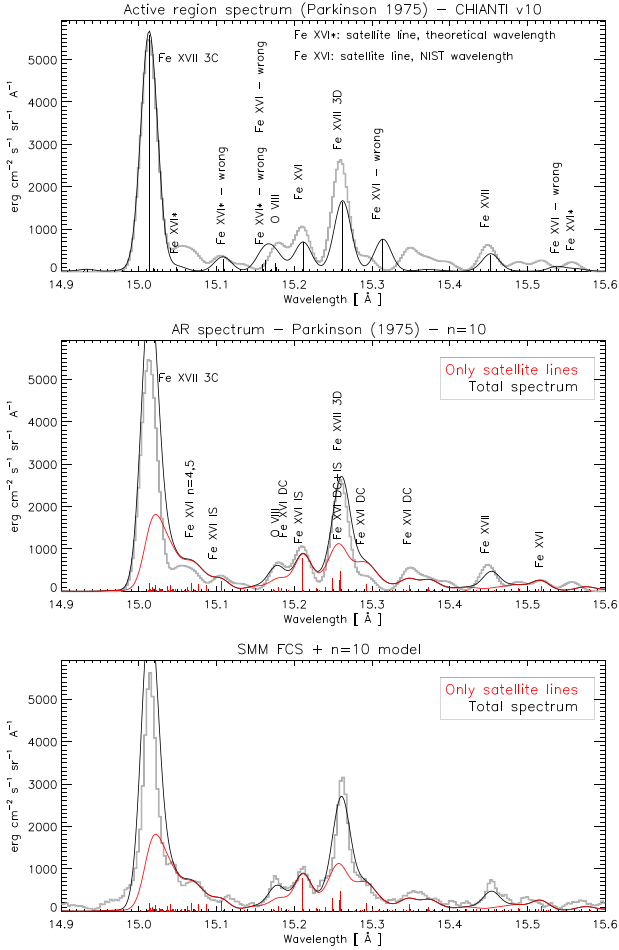
Figure 3. A comparison between the reconstructed P75 spectrum (grey thick line) and an averaged SMM/FCS spectrum of an active region with the CHIANTI v.10 data (top plot) and the present $n = 10$ model in the 15–15.6 Å region. The CHIANTI (NIST) wavelengths of the main lines are incorrect, with one exception. A few satellite lines mainly formed by IS excitation or DC are indicated.

wavelength is 15.54 Å. It could either be the solar line at 15.518 or that one at 15.557 Å, while B76 predicted, on an incorrect identification of the decay to the 3d $^2D_{5/2}$, a wavelength of 15.538 Å, where a solar line is not observed. We favour the first option, as the wavelength agrees with the Díaz et al. (2013) calculations, and its intensity is well matched. G09 has a predicted wavelength of 15.533 Å but gives an observed wavelength of 15.516 Å, despite the fact that there is no line clearly visible at that wavelength in their spectrum of Fig. 2.

Our model predicts many strong lines from the 2p^5 3d^2 configuration, which was not included by Liang et al. (2008). Such states were not considered by G09, as the lines are formed by DC. Surprisingly, such states were also not considered by B76. M05 list only two transitions, from $J = 5/2$ to 3d $^2D_{3/2}$ (Na2b, 15.360 Å), and from $J = 3/2$ to 3d $^2D_{3/2}$, at a predicted wavelength of 15.200 Å. In our model, we actually have two strong transitions from two nearby $J = 5/2$ states to the 3d $^2D_{3/2}$, at predicted wavelengths of 15.34 and 15.36 Å. They are likely blended to form the strong solar line at 15.348 Å. The model spectrum agrees very well with the P75 and FCS spectra. On the other hand, transitions from $J = 3/2$ to 3d $^2D_{3/2}$ are relatively weak in our model.

G09 found a blue wing around 15.19 Å and identified it with the transition 3–155 in their model, with a relative intensity of 0.18. The present model instead predicts a very weak relative intensity of 0.03. On the other hand, our model predicts two strong decays from the 2s^2 2p^5 3d^2 (5–211 and 5–210) which are most likely blending the 15.21 and 15.26 Å lines. We obtain a good agreement between predicted and observed spectra with these identifications. One of the two lines, the 5–211, was instead identified by M05 with a line in the Hercules spectra at 15.237 Å from a predicted wavelength of 15.225, although their spectra also have a strong line at 15.213 Å. The M05 identification is inconsistent with the present model, as there is no strong solar line at 15.237 Å.

We also identify a strong transition (3–152), with predicted wavelength of 15.30 Å with the solar one observed by P75 at 15.293 Å (plus a blend of $n = 5$ lines), considering that intensities and wavelengths match. This line is not listed by G09. What seems to be the same transition (Na3) was predicted by M05 to be at a very similar wavelength, 15.290 Å, but was actually identified with a line at 15.304 Å.

5.2 The satellites blending the 3C line at 15 Å

We note that the large number of transitions from $n = 4, 5$ states provide ab-initio wavelengths and intensities in broad agreement with the FCS observation. Several transitions from $n = 4, 5$ states are either blending the resonance line, or are scattered across many different spectral ranges.

The $n = 4$ satellites to the 3C line are mostly resolvable, being in the red wing, but the others are not. As previously mentioned, we have carried out a large-scale $n = 10$ calculation to improve the estimate of all the satellites of the 3C line. Most of the flux is due to transitions from $n = 4, 5$ states, but as Beiersdorfer et al. (2011) pointed out, some contribution from higher states is also present.

If one considers only the 2p^5 3d nl satellites within the Å 15.0– 15.06, which contribute about 75 per cent of the total flux in this band with the $n = 10$ model, the $n = 4, 5, 6$ states contribute most, with 16, 33, and 15 per cent, respectively. The $n = 7, 8, 9, 10$ states contribute progressively less: 9.5, 8.3, 5.3, and 3.9 per cent. Therefore, any missing flux due to even higher states would likely be at most a few per cent.

Finally, to assess the possible missing flux, we have carried out a configuration-averaged complete calculation including configurations up to $n = 30$. The wavelengths of the transitions are not very accurate, and if one considers decays from individual configurations some discrepancies are found with the totals from the j-resolved $n = 10$ model, hence comparisons between the calculations are not simple. If one considers the main transitions from the 2p^5 3d nl states, the $n = 30$ model indicates that those from the $n = 4 - 10$ states contribute 91 per cent, those from the $n = 11 - 20$ states 6 per cent, and those from the $n = 21 - 30$ states 3 per cent. However, the total flux within the 3C line from the $n = 30$ model is less than 2 per cent larger than what we calculated with the $n = 10$ model. Therefore, we conclude that any missing flux within the $n = 10$ model would amount only to a few per cent, in broad agreement with the Beiersdorfer et al. (2011) FAC result.

5.3 The 10–15 Å region

As shown in Fig. 4, our model predicts many transitions blending known transitions or explaining previously unidentified lines. Table 8 provides a short summary. There are many transitions from $n = 6$
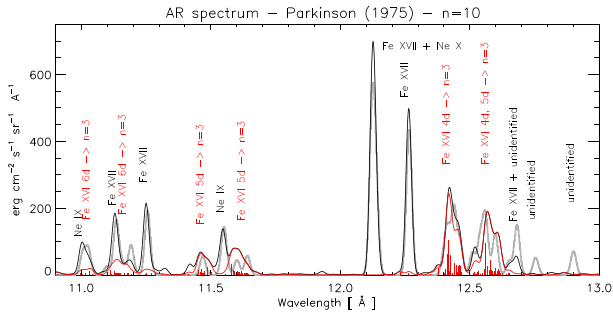
Figure 4. A comparison between the reconstructed P75 spectrum (grey thick line) and the present $n = 10$ model, indicating that several previously unidentified lines are due to Fe XVI. The red spectrum is the contribution from the satellite lines.

Table 8. List of newly identified satellite lines, Parkinson's KAP crystal.

λ_{obs}(Å)	Int	P75	upper
10.742	1.3	Ne IX	bl $n = 7,8$
11.006	1.7	Na X	bl $n = 6$
11.027	2.0	Ne IX	bl $n = 6$
11.099	0.7	Na X	bl $n = 6$
11.135	4.3	Fe XVII	bl $n = 5,6$
11.160	0.9	unid.	$n = 6$
11.192	2.4	Na X	$n = 4$
11.469	1.5	unid.	$n = 5$
11.601	1.2	unid.	$n = 5,6$
11.641	1.5	unid.	$n = 5$
12.399	1.2	unid.	$n = 4$
12.414	3.4	unid.	$n = 4$
12.439	5.2	unid.	$n = 4$
12.463	2.4	unid.	$n = 4$
12.510	1.8	unid.	$n = 4,5$
12.539	2.8	unid.	$n = 4,5$
12.560	4.7	unid.	$n = 4,5$
12.598	3.3	unid.	$n = 4,5$
12.651	1.1	Ni XIX	bl $n = 4,5$
13.868	2.1	unid.	$n = 4,5$
13.899	5.8	Fe XVII	bl $n = 3,4,5$
14.037	4.5	Ni XIX	bl $n = 3$
14.081	3.4	Ni XIX	bl $n = 3$
17.16	8.9	unid.	$n = 3$
17.21	12.	unid.	$n = 3$
17.40	7.9	unid.	$n = 3$
17.51	5.1	unid.	$n = 3$
17.77	5.4	O VII	bl $n = 3$

Note. The columns give the observed wavelengths, the radiance in erg cm^{-2} sr^{-1} s^{-1}, P75 identification (unid. for unidentified lines) and the upper states of the main satellite lines. bl indicates blending with satellite lines.

states that are blending known lines from Ne IX and Fe XVII between 11.0 and 11.3 Å. Within the 11.45 and 11.50 Å and 11.60 and 11.65 Å regions, our model predicts several decays from $2s^2\,2p^5\,3l\,5d$ states. Parkinson's spectrum has indeed unidentified transitions at 11.469, 11.601, and 11.641 with intensities similar to the predicted ones.

Within the 12.3 and 12.7 Å region, there are several relatively strong transitions from $2s^2\,2p^5\,3l\,4l'$, and some $n = 5$ states. Parkinson's spectrum has many unidentified transitions in this wavelength range. There is an excellent match between our ab-initio wavelengths and calculated intensities and the observed spectrum.

Several decays from $1s^2\,2s\,2p^6\,3p\,5f$, and 5g states are predicted between 13.8 and 13.9 Å and are blending the Fe XVII 13.899 Å line,

which is significantly underpredicted, and form the unidentified line at 13.868 Å.

Several transitions of the type $1s^2\,2s\,2p^6\,3l\,3l''$ predicted around 14.0 Å, are blending Ni XIX lines around 14.04 Å.

5.4 The 17–18 Å region

The situation for the weaker lines above 17 Å is rather unclear, as the calculations are more uncertain, and the sensitivity of the solar instruments was lower, hence only a few of the stronger lines were observed. G09 list various identifications for lines formed by IS excitation, but agreement with the observed spectrum is poor. P75 only lists four unidentified lines, at 17.151, 17.199, 17.389 (blended with O VII), and 17.501 Å. However, all the lines in Parkinson's spectrum above 16 Å have an incorrect wavelength, being lower by 0.01 Å. We have applied such correction to the spectra, see Table 8.

G09 lists several possible lines in the 17.37–17.42 Å range, a few others at 17.447 Å, and several others in the range 17.494–17.510 Å, i.e. effectively the laboratory spectrum has the same lines as the solar one (including a blend of emission for the first two lines). Our model also predicts many lines mostly formed by DC, but none that stand out for their brightness, so identifications are very difficult.

The brightest is a decay from 3s 3p $^4D_{7/2}$ (level No.38) to the 3p $^2P_{3/2}$, predicted at 17.63 Å. G09 has a similar predicted wavelength (17.619 Å), but gives an observed wavelength of 17.592 Å, which does not agree with the solar spectrum. D13 does not provide a calculated energy for the upper state, nor B76.

Similarly, there are several lines from low-lying states that our model predicts around 17.55 Å. The strongest of them, the decay of the 3s 3d $^4P_{5/2}$ to the 3d $^2D_{5/2}$, has a wavelength predicted by Liang et al. (2008) of 17.36 Å, but was instead identified by B76 with a line at 17.498 Å. Our identification agrees with G09.

6 CONCLUSIONS

Despite being a century from their discovery, satellite lines are still relatively poorly known. The literature on the identifications of the strongest lines is very confusing. Proper modelling requires large-scale calculations of accurate atomic data and further studies. From our brief summary of previous studies, both theoretical and experimental, it is clear that, especially for the satellite lines of Na-like iron, further studies are needed to benchmark the atomic data and to obtain experimental wavelengths. It is also clear that different theoretical approaches can provide significantly different models.

Such work is particularly important for Fe XVI as the satellite lines can be relatively strong and blend the Fe XVII 3C and 3D lines, which are among the most important X-ray lines, because of their plasma diagnostic use. We found that the missing flux around the 3C and 3D lines, about a factor of 2 as found from the analysis of the first MaGIXS flight, is mostly due to decays from AI states of Fe XVI.

We have also identified for the first time many other lines in the X-rays, and showed that some are also blending previously known lines. It is clear that a complete knowledge of these satellite lines is important when analysing astrophysical observations at these wavelengths, for example from the recently launched XRISM satellite. It is also clear that further calculations for other ions are needed.

Our comparison to the best available solar high-resolution spectra is very satisfactory, but further observations are needed to test the models. In this respect, the current NASA proposals for further sounding rockets with an improved MaGIXS instrument are very important.

DATA AVAILABILITY

The results of the largest $n = 10$ fine-structure resolved calculation are made available at ZENODO in CHIANTI version 11 ascii format, see https://doi.org/10.5281/zenodo.11474529. The IDL programs compatible with these files are available at https://github.com/CHIANTI-VIP/IDL/

REFERENCES

Aggarwal K. M., Keenan F. P., 2007, A&A, 463, 399
Badnell N. R., 2011, Comput. Phys. Commun., 182, 1528
Beiersdorfer P., Gu M. F., Lepson J., Desai P., 2011, in Johns-Krull C., Browning M. K., West A. A.eds, ASP Conf. Ser. Vol. 448, 16th Cambridge Workshop on Cool Stars, Stellar Systems, and the Sun. Astron. Soc. Pac., San Francisco, p. 787
Beiersdorfer P., Diaz F., Ishikawa Y., 2012, ApJ, 745, 167
Beiersdorfer P., Bode M. P., Ishikawa Y., Diaz F., 2014, ApJ, 793, 99
Beiersdorfer P., Hell N., Lepson J. K., 2018, ApJ, 864, 24
Berrington K. A., Eissner W. B., Norrington P. H., 1995, Comput. Phys. Commun., 92, 290
Brown G. V., Beiersdorfer P., Chen H., Chen M. H., Reed K. J., 2001, ApJ, 557, L75
Bruch R., Safronova U. I., Shlyaptseva A. S., Nilsen J., Schneider D., 1998, J. Quant. Spectrosc. Radiat. Transfer, 60, 605
Burkhalter P. G., Cohen L., Cowan R. D., Feldman U., 1979, J. Opt. Soc. Am., 69, 1133
Cohen L., Feldman U., 1970, ApJ, 160, L105
Cornille M., Dubau J., Faucher P., Bely-Dubau F., Blancard C., 1994, A&AS, 105, 77
Del Zanna G., 2011, A&A, 536, A59
Del Zanna G., Mason H. E., 2014, A&A, 565, A14
Del Zanna G., Mason H. E., 2018, Living Rev. Solar Phys., 15, 5
Del Zanna G., Dere K. P., Young P. R., Landi E., 2021, ApJ, 909, 38
Dere K. P., Del Zanna G., Young P. R., Landi E., Sutherland R. S., 2019, ApJS, 241, 22
Díaz F., Vilkas M. J., Ishikawa Y., Beiersdorfer P., 2013, ApJS, 207, 11
Dubau J., Volonte S., 1980, Rep. Prog. Phys., 43, 199
Gabriel A. H., 1972, MNRAS, 160, 99
Gabriel A. H., Paget T. M., 1972, J. Phys. B: At. Mol. Phys., 5, 673
Graf A., Beiersdorfer P., Brown G. V., Gu M. F., 2009, ApJ, 695, 818
Hummer D. G., Berrington K. A., Eissner W., Pradhan A. K., Saraph H. E., Tully J. A., 1993, A&A, 279, 298
Jupén C., Engström L., Hutton R., Träbert E., 1988, J. Phys. B: At. Mol. Phys., 21, L347
Kramida A., Ralchenko Yu., Reader J., NIST ASD Team, 2022, https://physics.nist.gov/asd, NIST Atomic Spectra Database (ver. 5.10), [Online]. Available: [2023, June 26]. National Institute of Standards and Technology, Gaithersburg, MD.
Kühn S. et al., 2022, Phys. Rev. Lett., 129, 245001
Liang G. Y., Badnell N. R., 2010, A&A, 518, A64 +
Liang Y., Whiteford A. D., Badnell N. R., 2008, J. Phys. B: At. Mol. Phys., 41, 235203
Loch S. D., Pindzola M. S., Ballance C. P., Griffin D. C., 2006, J. Phys. B: At. Mol. Phys., 39, 85

May M. J. et al., 2005, ApJS, 158, 230
Nilsen J., 1989, At. Data Nucl. Data Tables, 41, 131
Parkinson J. H., 1975, Sol. Phys., 42, 183 (P75)
Phillips K. J. H., Greer C. J., Bhatia A. K., Coffey I. H., Barnsley R., Keenan F. P., 1997, A&A, 324, 381
Quigley L., Berrington K., 1996, J. Phys. B: At. Mol. Phys., 29, 4529
Quigley L., Berrington K., Pelan J., 1998, Comput. Phys. Commun., 114, 225
Safronova U. I., Johnson W. R., Safronova M. S., Albritton J. R., 2002, Phys. Rev. A, 66, 052511
Savage S. L. et al., 2023, ApJ, 945, 105
Shirai T., Sugar J., Musgrove A., Wiese W., 2000, Spectral Data for Highly Ionized Atoms: Ti, V, Cr, Mn, Fe, Co, Ni, Cu, Kr, and Mo. J. Phys. Chem. Ref. Data, Monograph, Vol. 8, Am. Inst. Phys., Melville, NY

APPENDIX A: ADDITIONAL MATERIAL

Table A1 describes the target of the structure run of Liang et al (2008).
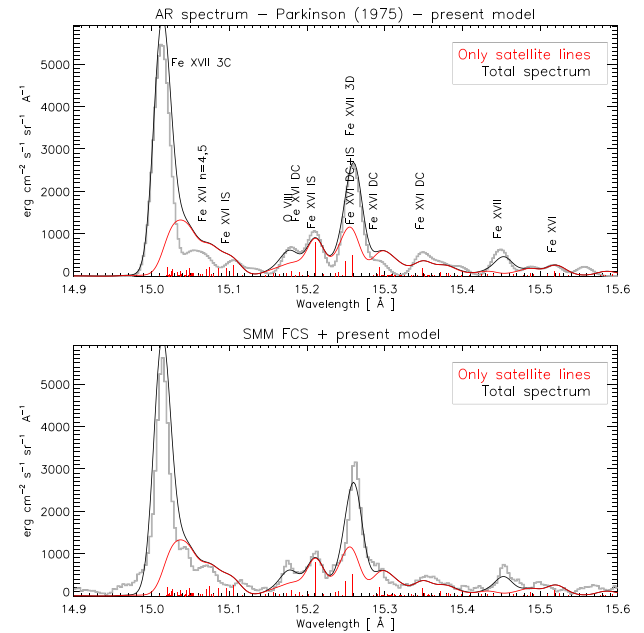
Figure A1. A comparison between the reconstructed P75 spectrum (grey thick line) and an averaged SMM/FCS spectrum of an active region with the present $n = 6$ model in the 15–15.6 Å region.

Table A1. The target electron configuration basis and orbital scaling parameters λ_{nl} for the structure run of Liang et al.

Configurations				
$1s^2\,2s^2\,2p^6\,3l\ (l = s,p,d)$	1s	1.39364		
$1s^2\,2s^2\,2p^5\,3l\,3l'\ (l = s,p,d,$	2s	1.08686	3s	1.15588
$l' = s,p)$				
	2p	1.02341	3p	1.11371
	3d	1.15100		

Table A2. List of the main states.

i	Conf.	P	T	$E_{\rm exp}$	$E_{\rm AS}$	$E_{\rm Diaz+}$	$E_{\rm Liang+}$
1	$2s^2\,2p^6\,3s$	e	$^2S_{1/2}$	0	0	0	0
2	$2s^2\,2p^6\,3p$	o	$^2P_{1/2}$	277194	276293	277222	276436
3	$2s^2\,2p^6\,3p$	o	$^2P_{3/2}$	298143	298373	298167	296534
4	$2s^2\,2p^6\,3d$	e	$^2D_{3/2}$	675501	674642	675463	676373
5	$2s^2\,2p^6\,3d$	e	$^2D_{5/2}$	678405	679275	678372	679712
77	$2s^2\,2p^5\,3s^2$	o	$^2P_{3/2}$	5773000?	5748000	5756556	5802584
78	$2s^2\,2p^5\,3s^2$	o	$^2P_{1/2}$	5873000?	5850943	5857665	5899697
79	$2s^2\,2p^5\,3s\,3p$	e	$^4S_{3/2}$	–	5941810	5953391	5991935
80	$2s^2\,2p^5\,3s\,3p$	e	$^4D_{5/2}$	5982000	5970059	5980479	6020272
81	$2s^2\,2p^5\,3s\,3p$	e	$^4D_{7/2}$	–	5976391	5986775	6026148
82	$2s^2\,2p^5\,3s\,3p$	e	$^2P_{3/2}$	–	5977178	5987047	6027021
83	$2s^2\,2p^5\,3s\,3p$	e	$^2P_{1/2}$	6001000	5989400	5999543	6041011
84	$2s^2\,2p^5\,3s\,3p$	e	$^4P_{5/2}$	6013000	6001435	6011855	6053544
85	$2s^2\,2p^5\,3s\,3p$	e	$^2D_{3/2}$	6013000	6002818	6012375	6053898
86	$2s^2\,2p^5\,3s\,3p$	e	$^2S_{1/2}$	6042000?	6019309	6027754	6076536
87	$2s^2\,2p^5\,3s\,3p$	e	$^4D_{1/2}$	6075000	6068977	6077192	6113566
88	$2s^2\,2p^5\,3s\,3p$	e	$^4P_{1/2}$	6089000?	6074866	6082835	6128206
89	$2s^2\,2p^5\,3s\,3p$	e	$^4D_{3/2}$	6089000	6079784	6087509	6124285
90	$2s^2\,2p^5\,3s\,3p$	e	$^2D_{5/2}$	6090463	6096282	6096282	6141431
91	$2s^2\,2p^5\,3s\,3p$	e	$^4P_{3/2}$	6096000	6091914	6100268	6138528
92	$2s^2\,2p^5\,3s\,3p$	e	$^2D_{5/2}$	6110000	6101305	6108077	6147237
93	$2s^2\,2p^5\,3s\,3p$	e	$^2P_{3/2}$	6129000	6108503	6113831	6157761
94	$2s^2\,2p^5\,3s\,3p$	e	$^2P_{1/2}$	–	6181158	6182346	6229457
95	$2s^2\,2p^5\,3s\,3p$	e	$^2D_{3/2}$	6217000?	6198457	6201702	6244142
96	$2s^2\,2p^5\,3s\,3p$	e	$^2S_{1/2}$	6267000?	6253611	6245187	6313279
111	$2s^2\,2p^5\,3s\,3d$	o	$^4P_{5/2}$	6393000	6382976	6390567	6440048
112	$2s^2\,2p^5\,3s\,3d$	o	$^4F_{9/2}$	–	6383060	6389221	6438162
117	$2s^2\,2p^5\,3s\,3d$	o	$^4F_{5/2}$	6406000	6397726	6404701	6453145
118	$2s^2\,2p^5\,3p^2$	o	$^2P_{3/2}$	–	6400493	6406003	6469670
119	$2s^2\,2p^5\,3s\,3d$	o	$^2D_{3/2}$	6419000	6408540	6415660	6464402
120	$2s^2\,2p^5\,3p^2$	o	$^2D_{3/2}$	–	6415643	6422064	6455698
121	$2s^2\,2p^5\,3s\,3d$	o	$^4D_{7/2}$	6422000	6416259	6421329	6471649
122	$2s^2\,2p^5\,3p^2$	o	$^2D_{5/2}$	–	6418038	6423498	6464730
123	$2s^2\,2p^5\,3s\,3d$	o	$^2P_{1/2}$	6423000	6418066	6423578	6476262
124	$2s^2\,2p^5\,3s\,3d$	o	$^2F_{5/2}$	6425000	6420114	6425339	6474699
125	$2s^2\,2p^5\,3s\,3d$	o	$^2P_{3/2}$	6436000	6439623	6443091	6498398
				6444100?			

Table A2 – *continued*

i	Conf.	P	T	$E_{\rm exp}$	$E_{\rm AS}$	$E_{\rm Diaz+}$	$E_{\rm Liang+}$
126	$2s^2\,2p^5\,3s\,3d$	o	$^4D_{1/2}$	–	6450153	6455202	6506414
127	$2s^2\,2p^5\,3s\,3d$	o	$^4D_{3/2}$	6473000	6479009	6483365	6536053
128	$2s^2\,2p^5\,3s\,3d$	o	$^2F_{7/2}$	6445000	6483824	6485011	6546990
129	$2s^2\,2p^5\,3s\,3d$	o	$^4F_{3/2}$	6502000	6496562	6502061	6547383
130	$2s^2\,2p^5\,3s\,3d$	o	$^2D_{5/2}$	6464000	6498874	6501608	6555370
131	$2s^2\,2p^5\,3s\,3d$	o	$^4D_{5/2}$	6502000	6499710	6504077	6549706
132	$2s^2\,2p^5\,3p^2$	o	$^2P_{1/2}$	–	6507356	6508883	6566725
133	$2s^2\,2p^5\,3s\,3d$	o	$^2D_{5/2}$	6516000	6511948	6514575	6569938
134	$2s^2\,2p^5\,3s\,3d$	o	$^2F_{7/2}$	6517000	6512092	6514871	6561652
135	$2s^2\,2p^5\,3p^2$	o	$^2P_{1/2}$	–	6512966	6514341	6579688
136	$2s^2\,2p^5\,3p^2$	o	$^2P_{3/2}$	–	6530425	6531608	6592253
137	$2s^2\,2p^5\,3s\,3d$	o	$^2D_{3/2}$	6530000	6551020	6550184	6611638
				6553500?			
138	$2s^2\,2p^5\,3s\,3d$	o	$^2P_{1/2}$	6574000	6576810	6573657	6644694
139	$2s^2\,2p^5\,3p^2$	e	$^4D_{1/2}$	–	6589929	6601400	6646599
140	$2s^2\,2p^5\,3s\,3d$	o	$^2F_{5/2}$	6556000	6594116	6593543	6651977
141	$2s^2\,2p^5\,3p\,3d$	e	$^4D_{3/2}$	–	6598110	6608991	6654887
142	$2s^2\,2p^5\,3p\,3d$	e	$^4D_{5/2}$	–	6610901	6620899	6667902
143	$2s^2\,2p^5\,3s\,3d$	o	$^2P_{3/2}$	6595000	6619300	6616740	6686516
				6620000?			
195	$2s^2\,2p^5\,3p\,3d$	e	$^2D_{3/2}$	6831000?	6834145	6831282	6894915
196	$2s^2\,2p^5\,3p\,3d$	e	$^2D_{5/2}$	6837100?	6839169	6838045	6893483
235	$2s^2\,2p^5\,3d^2$	o	$^2G_{7/2}$	7135000?	7132714	7134361	–
236	$2s^2\,2p^5\,3d^2$	o	$^4F_{5/2}$	–	7139463	7142053	–
237	$2s\,2p^6\,3s\,3p$	o	$^2P_{3/2}$	–	7140998	7128949	–
244	$2s^2\,2p^5\,3d^2$	o	$^2F_{5/2}$	**7180800?**	7185725	7186088	–
245	$2s^2\,2p^5\,3d^2$	o	$^2F_{7/2}$	**7191000?**	7190776	7193832	–
254	$2s^2\,2p^5\,3d^2$	o	$^2F_{7/2}$	**7236000?**	7243251	7242818	–
255	$2s^2\,2p^5\,3d^2$	o	$^2D_{5/2}$	**7240000?**	7252103	7246119	–
256	$2s^2\,2p^5\,3d^2$	o	$^2D_{3/2}$	–	7258926	7253388	–
257	$2s^2\,2p^5\,3d^2$	o	$^2P_{3/2}$	**7266000?**	7270449	7263947	–

Note. $E_{\rm exp}$ gives the NIST experimental energies, except the those in bold which are our tentative values. $E_{\rm AS}$ are our ab-initio AS energies with the $n = 10$ model. $E_{\rm Diaz+}$ are the energies from Díaz et al. (2013), while $E_{\rm Liang+}$ are the AS ones from Liang et al. (2008).

Table A3. Energies.

i	Conf.	P	T	E_{NIST}	E_{AS}	E_{Diaz+}	E_{Liang+}
1	$2s^2\,2p^6\,3s$	e	$^2S_{1/2}$	0	0	0	0
2	$2s^2\,2p^6\,3p$	o	$^2P_{1/2}$	277194	277711	277222	276436
3	$2s^2\,2p^6\,3p$	o	$^2P_{3/2}$	298143	300089	298167	296534
4	$2s^2\,2p^6\,3d$	e	$^2D_{3/2}$	675501	676579	675463	676373
5	$2s^2\,2p^6\,3d$	e	$^2D_{5/2}$	678405	681330	678372	679712
6	$2s^2\,2p^6\,4s$	e	$^2S_{1/2}$	1867740	1869087	1867664	1867895
7	$2s^2\,2p^6\,4p$	o	$^2P_{1/2}$	1977649	1979132	1977616	1977070
8	$2s^2\,2p^6\,4p$	o	$^2P_{3/2}$	1985649	1987870	1985786	1984703
9	$2s^2\,2p^6\,4d$	e	$^2D_{3/2}$	2124719	2126589	2124584	2124092
10	$2s^2\,2p^6\,4d$	e	$^2D_{5/2}$	2125959	2128787	2125923	2125524
11	$2s^2\,2p^6\,4f$	o	$^2F_{5/2}$	2184960	2184613	2184910	2184919
12	$2s^2\,2p^6\,4f$	o	$^2F_{7/2}$	2185409	2185387	2185401	2185424
13	$2s^2\,2p^6\,5s$	e	$^2S_{1/2}$	2662000	2663585	2663328	2662751
14	$2s^2\,2p^6\,5p$	o	$^2P_{1/2}$	2717169	2717783	2717620	2716785
15	$2s^2\,2p^6\,5p$	o	$^2P_{3/2}$	2721159	2722230	2721636	2720472
16	$2s^2\,2p^6\,5d$	e	$^2D_{3/2}$	2788049	2789109	2788713	2787715
17	$2s^2\,2p^6\,5d$	e	$^2D_{5/2}$	2788609	2790271	2789416	2788448
18	$2s^2\,2p^6\,5f$	o	$^2F_{5/2}$	2818599	2818306	2818974	2818342
19	$2s^2\,2p^6\,5f$	o	$^2F_{7/2}$	2818900	2818714	2819226	2818601
20	$2s^2\,2p^6\,5g$	e	$^2G_{7/2}$	2822700	2821171	0	2821317
21	$2s^2\,2p^6\,5g$	e	$^2G_{9/2}$	2822800	2821402	0	2821470
22	$2s^2\,2p^6\,6s$	e	$^2S_{1/2}$	3075999	3075706	0	3075119
23	$2s^2\,2p^6\,6p$	o	$^2P_{1/2}$	3106400	3106229	0	3105599
24	$2s^2\,2p^6\,6p$	o	$^2P_{3/2}$	3108899	3108902	–	3107635
25	$2s^2\,2p^6\,6d$	e	$^2D_{3/2}$	3146070	3146303	–	3145288
26	$2s^2\,2p^6\,6d$	e	$^2D_{5/2}$	3146670	3147021	–	3145709
27	$2s^2\,2p^6\,6f$	o	$^2F_{5/2}$	3163129	3162874	–	3162816
28	$2s^2\,2p^6\,6f$	o	$^2F_{7/2}$	3163190	3163122	–	3162966
29	$2s^2\,2p^6\,6g$	e	$^2G_{7/2}$	–	3164672	–	3164757
30	$2s^2\,2p^6\,6g$	e	$^2G_{9/2}$	–	3164807	–	3164846
31	$2s^2\,2p^6\,6h$	o	$^2H_{9/2}$	–	3164858	–	3164916
32	$2s^2\,2p^6\,6h$	o	$^2H_{11/2}$	–	3164947	–	3164976
33	$2s^2\,2p^5\,3s^2$	o	$^2P_{3/2}$	5773000?	5744641	5756556	5802584
34	$2s^2\,2p^5\,3s^2$	o	$^2P_{1/2}$	5873000?	5848114	5857665	5899697
35	$2s^2\,2p^5\,3s\,3p$	e	$^4S_{3/2}$	–	5939043	5953391	5991935
36	$2s^2\,2p^5\,3s\,3p$	e	$^4D_{5/2}$	5982000	5967095	5980479	6020272
37	$2s^2\,2p^5\,3s\,3p$	e	$^4D_{7/2}$	–	5973428	5986775	6026148
38	$2s^2\,2p^5\,3s\,3p$	e	$^2P_{3/2}$	–	5974184	5987047	6027021
39	$2s^2\,2p^5\,3s\,3p$	e	$^2P_{1/2}$	6001000	5986456	5999543	6041011
40	$2s^2\,2p^5\,3s\,3p$	e	$^4P_{5/2}$	6013000	5998400	6011855	6053544
41	$2s^2\,2p^5\,3s\,3p$	e	$^2D_{3/2}$	6013000	5999767	6012375	6053898
42	$2s^2\,2p^5\,3s\,3p$	e	$^2S_{1/2}$	6042000?	6016544	6027754	6076536
43	$2s^2\,2p^5\,3s\,3p$	e	$^4D_{1/2}$	6075000	6066510	6077192	6113566
44	$2s^2\,2p^5\,3s\,3p$	e	$^4P_{1/2}$	6089000?	6072233	6082835	6128206
45	$2s^2\,2p^5\,3s\,3p$	e	$^4D_{3/2}$	6089000	6077288	6087509	6124285
46	$2s^2\,2p^5\,3s\,3p$	e	$^2D_{5/2}$	–	6087412	6096282	6141431
47	$2s^2\,2p^5\,3s\,3p$	e	$^4P_{3/2}$	6096000	6089389	6100268	6138528
48	$2s^2\,2p^5\,3s\,3p$	e	$^2D_{5/2}$	6110000	6098693	6108077	6147237
49	$2s^2\,2p^5\,3s\,3p$	e	$^2P_{3/2}$	6129000?	6105380	6113831	6157761
50	$2s^2\,2p^5\,3s\,3p$	e	$^2P_{1/2}$	–	6178837	6182346	6229457
51	$2s^2\,2p^5\,3s\,3p$	e	$^2D_{3/2}$	6217000?	6195854	6201702	6244142
52	$2s^2\,2p^5\,3s\,3p$	e	$^2S_{1/2}$	6267000?	6252510	6245187	6313279
53	$2s^2\,2p^5\,3p^2$	o	$^4P_{3/2}$	–	6257463	6269659	6316508
54	$2s^2\,2p^5\,3p^2$	o	$^2P_{1/2}$	–	6258792	6271517	6317822
55	$2s^2\,2p^5\,3p^2$	o	$^4P_{5/2}$	–	6265662	6278181	6324087
56	$2s^2\,2p^5\,3p^2$	o	$^2F_{7/2}$	–	6276200	6287623	6328785
57	$2s^2\,2p^5\,3p^2$	o	$^2P_{3/2}$	–	6278747	6291100	6334949
58	$2s^2\,2p^5\,3p^2$	o	$^4P_{1/2}$	–	6295965	6307896	6353532
59	$2s^2\,2p^5\,3p^2$	o	$^2D_{5/2}$	–	6297314	6308932	6350782
60	$2s^2\,2p^5\,3p^2$	o	$^2D_{3/2}$	–	6298455	6308901	6352715
61	$2s^2\,2p^5\,3p^2$	o	$^4D_{7/2}$	–	6303014	6314133	6356554
62	$2s^2\,2p^5\,3p^2$	o	$^4D_{5/2}$	–	6304417	6315498	6358568
63	$2s^2\,2p^5\,3p^2$	o	$^4D_{1/2}$	–	6353354	6362006	6404267
64	$2s^2\,2p^5\,3s\,3d$	o	$^4P_{1/2}$	–	6356616	6369713	6418318

Table A3 – *continued*

i	Conf.	P	T	E_NIST	E_{AS}	$E_\mathrm{Diaz+}$	$E_\mathrm{Liang+}$
65	$2s^2\,2p^5\,3p^2$	o	$^4S_{3/2}$	–	6357933	6368079	6411844
66	$2s^2\,2p^5\,3s\,3d$	o	$^4P_{3/2}$	–	6365097	6377262	6426196
67	$2s^2\,2p^5\,3s\,3d$	o	$^4P_{5/2}$	6393000	6379612	6390567	6440048
68	$2s^2\,2p^5\,3s\,3d$	o	$^4F_{9/2}$	–	6379790	6389221	6438162
69	$2s^2\,2p^5\,3p^2$	o	$^4D_{3/2}$	–	6381562	6390640	6432092
70	$2s^2\,2p^5\,3p^2$	o	$^2F_{5/2}$	–	6385341	6394058	6431790
71	$2s^2\,2p^5\,3s\,3d$	o	$^4F_{7/2}$	–	6385866	6396084	6444453
72	$2s^2\,2p^5\,3p^2$	o	$^2S_{1/2}$	–	6390585	6398771	6439224
73	$2s^2\,2p^5\,3s\,3d$	o	$^4F_{5/2}$	6406000	6394429	6404701	6453145
74	$2s^2\,2p^5\,3p^2$	o	$^2P_{3/2}$	–	6397961	6406003	6469670
75	$2s^2\,2p^5\,3s\,3d$	o	$^2D_{3/2}$	6419000	6405385	6415660	6464402
76	$2s^2\,2p^5\,3p^2$	o	$^2D_{3/2}$	–	6413008	6422064	6455698
77	$2s^2\,2p^5\,3s\,3d$	o	$^4D_{7/2}$	6422000	6413123	6421329	6471649
78	$2s^2\,2p^5\,3s\,3d$	o	$^2P_{1/2}$	–	6415027	6423498	6464730
79	$2s^2\,2p^5\,3s\,3d$	o	$^2F_{5/2}$	6423000	6415181	6423578	6476262
80	$2s^2\,2p^5\,3p^2$	o	$^2D_{5/2}$	6425000	6417371	6425339	6474699
81	$2s^2\,2p^5\,3s\,3d$	o	$^2P_{3/2}$	<u>6436000</u>	6436676	6443091	6498398
				6444100?			
82	$2s^2\,2p^5\,3s\,3d$	o	$^4D_{1/2}$	–	6447867	6455202	6506414
83	$2s^2\,2p^5\,3s\,3d$	o	$^4D_{3/2}$	<u>6473000</u>	6476481	6483365	6536053
84	$2s^2\,2p^5\,3s\,3d$	o	$^2F_{7/2}$	<u>6445000</u>	6480673	6485011	6546990
85	$2s^2\,2p^5\,3s\,3d$	o	$^4F_{3/2}$	6502000	6493786	6502061	6547383
86	$2s^2\,2p^5\,3s\,3d$	o	$^2D_{5/2}$	<u>6464000</u>	6495941	6501608	6549706
87	$2s^2\,2p^5\,3s\,3d$	o	$^4D_{5/2}$	6502000	6496993	6504077	6555370
88	$2s^2\,2p^5\,3p^2$	o	$^2P_{1/2}$	–	6504938	6508883	6566725
89	$2s^2\,2p^5\,3s\,3d$	o	$^2D_{5/2}$	6516000	6508973	6514575	6569938
90	$2s^2\,2p^5\,3s\,3d$	o	$^2F_{7/2}$	6517000	6509407	6514871	6561652
91	$2s^2\,2p^5\,3p^2$	o	$^2P_{1/2}$	–	6511585	6514341	6579688
92	$2s^2\,2p^5\,3p^2$	o	$^2P_{3/2}$	–	6528784	6531608	6592253
93	$2s^2\,2p^5\,3s\,3d$	o	$^2D_{3/2}$	<u>6530000</u>	6549199	6550184	6611638
				6553500?			
94	$2s^2\,2p^5\,3s\,3d$	o	$^2P_{1/2}$	6574000	6575409	6573657	6644694
95	$2s^2\,2p^5\,3p\,3d$	e	$^4D_{1/2}$	–	6586884	6601400	6646599
96	$2s^2\,2p^5\,3s\,3d$	o	$^2F_{5/2}$	<u>6556000</u>	6591507	6593543	6651977
97	$2s^2\,2p^5\,3p\,3d$	e	$^4D_{3/2}$	–	6595119	6608991	6654887
98	$2s^2\,2p^5\,3p\,3d$	e	$^4D_{5/2}$	–	6607993	6620899	6667902
99	$2s^2\,2p^5\,3s\,3d$	o	$^2P_{3/2}$	<u>6595000</u>	6617260	6616740	6686516
				6620000?			
100	$2s^2\,2p^5\,3p\,3d$	e	$^4D_{7/2}$	–	6623086	6634662	6682013
101	$2s^2\,2p^5\,3p\,3d$	e	$^4G_{7/2}$	–	6629973	6640658	6685459
102	$2s^2\,2p^5\,3p\,3d$	e	$^4G_{9/2}$	–	6631373	6641641	6685281
103	$2s^2\,2p^5\,3p\,3d$	e	$^2D_{5/2}$	–	6634688	6645828	6692155
104	$2s^2\,2p^5\,3p\,3d$	e	$^4G_{11/2}$	–	6636164	6646042	6690008
105	$2s^2\,2p^5\,3p\,3d$	e	$^2D_{3/2}$	–	6639303	6650162	6696538
106	$2s^2\,2p^5\,3p\,3d$	e	$^4G_{5/2}$	–	6649416	6659988	6704606
107	$2s^2\,2p^5\,3p\,3d$	e	$^2F_{7/2}$	–	6650899	6660419	6704344
108	$2s^2\,2p^5\,3p\,3d$	e	$^2P_{1/2}$	–	6652928	6664075	6708793
109	$2s^2\,2p^5\,3p\,3d$	e	$^4P_{1/2}$	–	6661688	6673499	6721372
110	$2s^2\,2p^5\,3p\,3d$	e	$^2G_{7/2}$	–	6663503	6673065	6718402
111	$2s^2\,2p^5\,3p\,3d$	e	$^4P_{3/2}$	–	6666392	6678388	6725771
112	$2s^2\,2p^5\,3p\,3d$	e	$^4F_{9/2}$	–	6675064	6684395	6729992
113	$2s^2\,2p^5\,3p\,3d$	e	$^4P_{5/2}$	–	6676103	6686826	6736070
114	$2s^2\,2p^5\,3p\,3d$	e	$^4S_{3/2}$	–	6676694	6686155	6731171
115	$2s^2\,2p^5\,3p\,3d$	e	$^4D_{7/2}$	–	6678774	6688328	6733893
116	$2s^2\,2p^5\,3p\,3d$	e	$^4D_{5/2}$	–	6679065	6689006	6735168
117	$2s^2\,2p^5\,3p\,3d$	e	$^4P_{3/2}$	–	6686282	6696202	6742881
118	$2s^2\,2p^5\,3p\,3d$	e	$^4F_{3/2}$	–	6692732	6701502	6747267
119	$2s^2\,2p^5\,3p\,3d$	e	$^4F_{9/2}$	–	6693560	6701731	6747879
120	$2s^2\,2p^5\,3p\,3d$	e	$^4D_{5/2}$	–	6701323	6708959	6755032
121	$2s^2\,2p^5\,3p\,3d$	e	$^4F_{7/2}$	–	6701728	6710310	6756669
122	$2s^2\,2p^5\,3p\,3d$	e	$^2F_{5/2}$	–	6703862	6712468	6759091

Table A3 – *continued*

i	Conf.	P	T	E_{NIST}	E_{AS}	E_{Diaz+}	E_{Liang+}
123	$2s^2\,2p^5\,3p\,3d$	e	$^2P_{1/2}$	–	6706716	6716454	6762890
124	$2s^2\,2p^5\,3p\,3d$	e	$^4D_{7/2}$	–	6708705	6716199	6762469
125	$2s^2\,2p^5\,3p\,3d$	e	$^2D_{3/2}$	–	6716985	6725873	6772014
126	$2s^2\,2p^5\,3p\,3d$	e	$^4F_{5/2}$	–	6719573	6727671	6774524
127	$2s^2\,2p^5\,3p\,3d$	e	$^2D_{3/2}$	–	6721823	6729273	6779084
128	$2s^2\,2p^5\,3p\,3d$	e	$^2F_{5/2}$	–	6727098	6735550	6776322
129	$2s^2\,2p^5\,3p\,3d$	e	$^4D_{1/2}$	–	6735806	6741753	6791670
130	$2s^2\,2p^5\,3p\,3d$	e	$^2F_{5/2}$	–	6736348	6743324	6789725
131	$2s^2\,2p^5\,3p\,3d$	e	$^2S_{1/2}$	–	6741107	6748420	6798866
132	$2s^2\,2p^5\,3p\,3d$	e	$^2D_{3/2}$	–	6741255	6749251	6794915
133	$2s^2\,2p^5\,3p\,3d$	e	$^4F_{7/2}$	–	6748758	6756215	6796906
134	$2s^2\,2p^5\,3p\,3d$	e	$^2F_{5/2}$	–	6753395	6760746	6802029
135	$2s^2\,2p^5\,3p\,3d$	e	$^2F_{7/2}$	–	6762854	6770538	6812665
136	$2s^2\,2p^5\,3p\,3d$	e	$^2G_{9/2}$	–	6765819	6771871	6818324
137	$2s^2\,2p^5\,3p\,3d$	e	$^4D_{3/2}$	–	6765828	6771678	6815497
138	$2s^2\,2p^5\,3p\,3d$	e	$^2G_{9/2}$	–	6768948	6772828	6826856
139	$2s^2\,2p^5\,3p\,3d$	e	$^4F_{3/2}$	–	6774024	6780566	6827080
140	$2s^2\,2p^5\,3p\,3d$	e	$^4P_{5/2}$	–	6780018	6784892	6837175
141	$2s^2\,2p^5\,3p\,3d$	e	$^4P_{1/2}$	–	6789682	6795392	6847309
142	$2s^2\,2p^5\,3p\,3d$	e	$^2F_{7/2}$	–	6790910	6794465	6849062
143	$2s^2\,2p^5\,3p\,3d$	e	$^2D_{5/2}$	–	6794015	6799158	6844589
144	$2s^2\,2p^5\,3p\,3d$	e	$^2D_{5/2}$	–	6799905	6804620	6854237
145	$2s^2\,2p^5\,3p\,3d$	e	$^2P_{3/2}$	–	6800872	6806274	6850264
146	$2s^2\,2p^5\,3p\,3d$	e	$^4D_{3/2}$	–	6805430	6812168	6855813
147	$2s^2\,2p^5\,3p\,3d$	e	$^4D_{1/2}$	–	6805751	6813392	6855558
148	$2s^2\,2p^5\,3p\,3d$	e	$^2F_{7/2}$	–	6809574	6812846	6865703
149	$2s^2\,2p^5\,3p\,3d$	e	$^2P_{3/2}$	–	6809716	6814230	6858541
150	$2s^2\,2p^5\,3p\,3d$	e	$^4F_{5/2}$	–	6811249	6815936	6861713
151	$2s^2\,2p^5\,3p\,3d$	e	$^2D_{3/2}$	**6831000?**	6833056	6831282	6894915
152	$2s^2\,2p^5\,3p\,3d$	e	$^2D_{5/2}$	**6837100?**	6837436	6838045	6893483
153	$2s^2\,2p^5\,3p\,3d$	e	$^2P_{1/2}$	–	6840857	6841603	6897847
154	$2s^2\,2p^5\,3p\,3d$	e	$^2P_{3/2}$	–	6859775	6859383	6918774
155	$2s\,2p^6\,3s^2$	e	$^2S_{1/2}$	–	6869901	6861675	–
156	$2s^2\,2p^5\,3p\,3d$	e	$^2P_{1/2}$	–	6883420	6878831	6941928
157	$2s^2\,2p^5\,3p\,3d$	e	$^2G_{7/2}$	–	6883442	6884423	6936104
158	$2s^2\,2p^5\,3p\,3d$	e	$^2D_{5/2}$	–	6894168	6888882	6952863
159	$2s^2\,2p^5\,3p\,3d$	e	$^2P_{3/2}$	–	6897773	6894592	6954817
160	$2s^2\,2p^5\,3p\,3d$	e	$^2S_{1/2}$	–	6915372	6913088	6972752
161	$2s^2\,2p^5\,3p\,3d$	e	$^2D_{3/2}$	–	6928727	6920217	6995240
162	$2s^2\,2p^5\,3p\,3d$	e	$^2D_{5/2}$	–	6935337	6926090	7004293
163	$2s^2\,2p^5\,3d^2$	o	$^4D_{1/2}$	–	7025231	7037203	–
164	$2s^2\,2p^5\,3d^2$	o	$^4D_{3/2}$	–	7028016	7039419	–
165	$2s^2\,2p^5\,3d^2$	o	$^4D_{5/2}$	–	7032672	7043009	–
166	$2s^2\,2p^5\,3d^2$	o	$^4D_{7/2}$	–	7040652	7049523	–
167	$2s^2\,2p^5\,3d^2$	o	$^4G_{11/2}$	–	7048994	7055594	–
168	$2s^2\,2p^5\,3d^2$	o	$^4G_{9/2}$	–	7050157	7058175	–
169	$2s^2\,2p^5\,3d^2$	o	$^4G_{7/2}$	–	7055533	7064132	–
170	$2s^2\,2p^5\,3d^2$	o	$^2F_{5/2}$	–	7055676	7064629	–
171	$2s\,2p^6\,3s\,3p$	o	$^4P_{1/2}$	–	7064005	7058900	–
172	$2s^2\,2p^5\,3d^2$	o	$^4P_{5/2}$	–	7066685	7074576	–
173	$2s^2\,2p^5\,3d^2$	o	$^4F_{9/2}$	–	7067562	7073220	–
174	$2s^2\,2p^5\,3d^2$	o	$^2G_{7/2}$	–	7068720	7075094	–
175	$2s^2\,2p^5\,3d^2$	o	$^2D_{3/2}$	–	7069932	7078209	–
176	$2s\,2p^6\,3s\,3p$	o	$^4P_{3/2}$	–	7070546	7065086	–
177	$2s^2\,2p^5\,3d^2$	o	$^2D_{5/2}$	–	7076759	7081804	–
178	$2s^2\,2p^5\,3d^2$	o	$^4P_{3/2}$	–	7078608	7086971	–
179	$2s\,2p^6\,3s\,3p$	o	$^4P_{5/2}$	–	7083684	7078148	–
180	$2s^2\,2p^5\,3d^2$	o	$^2P_{1/2}$	–	7086134	7092704	–
181	$2s^2\,2p^5\,3d^2$	o	$^2H_{11/2}$	–	7087677	7091469	–
182	$2s^2\,2p^5\,3d^2$	o	$^2F_{7/2}$	–	7094562	7099854	–
183	$2s^2\,2p^5\,3d^2$	o	$^4D_{5/2}$	–	7094609	7101485	–
184	$2s^2\,2p^5\,3d^2$	o	$^4F_{3/2}$	–	7097492	7103859	–
185	$2s^2\,2p^5\,3d^2$	o	$^4D_{7/2}$	–	7098186	7104169	–

Table A3 – *continued*

i	Conf.	P	T	E_{NIST}	E_{AS}	$E_{\text{Diaz+}}$	$E_{\text{Liang+}}$
186	$2s^2\,2p^5\,3d^2$	o	$^4P_{1/2}$	–	7099272	7104271	–
187	$2s^2\,2p^5\,3d^2$	o	$^2G_{9/2}$	–	7114444	7118468	–
188	$2s^2\,2p^5\,3d^2$	o	$^4G_{5/2}$	–	7117849	7124454	–
189	$2s^2\,2p^5\,3d^2$	o	$^2D_{3/2}$	–	7124454	7128734	–
190	$2s\,2p^6\,3s\,3p$	o	$^2P_{1/2}$	–	7127309	7116914	–
191	$2s^2\,2p^5\,3d^2$	o	$^2G_{7/2}$	**7135000?**	7130233	7134361	–
192	$2s^2\,2p^5\,3d^2$	o	$^4F_{5/2}$	–	7136863	7142053	–
193	$2s\,2p^6\,3s\,3p$	o	$^2P_{3/2}$	–	7138849	7128949	–
194	$2s^2\,2p^5\,3d^2$	o	$^4S_{3/2}$	–	7145140	7148076	–
195	$2s^2\,2p^5\,3d^2$	o	$^4F_{7/2}$	–	7159683	7163088	–
196	$2s^2\,2p^5\,3d^2$	o	$^4D_{1/2}$	–	7160005	7165078	–
197	$2s^2\,2p^5\,3d^2$	o	$^2G_{9/2}$	–	7169545	7172806	–
198	$2s^2\,2p^5\,3d^2$	o	$^2P_{3/2}$	–	7181008	7183471	–
199	$2s^2\,2p^5\,3d^2$	o	$^2F_{7/2}$	–	7182632	7185214	–
200	$2s^2\,2p^5\,3d^2$	o	$^2F_{5/2}$	**7180800?**	7183602	7186088	–
201	$2s^2\,2p^5\,3d^2$	o	$^2F_{5/2}$	**7191000?**	7188617	7193832	–
202	$2s^2\,2p^5\,3d^2$	o	$^2S_{1/2}$	–	7200182	7199268	–
203	$2s^2\,2p^5\,3d^2$	o	$^4D_{3/2}$	–	7200476	7203616	–
204	$2s^2\,2p^5\,3d^2$	o	$^2H_{9/2}$	–	7207565	7209123	–
205	$2s^2\,2p^5\,3d^2$	o	$^2D_{5/2}$	–	7210871	7211689	–
206	$2s\,2p^6\,3s\,3p$	o	$^2P_{1/2}$	–	7212169	7199268	–
207	$2s^2\,2p^5\,3d^2$	o	$^2P_{3/2}$	–	7214311	7211685	–
208	$2s\,2p^6\,3s\,3p$	o	$^2P_{3/2}$	–	7216411	7203904	–
209	$2s^2\,2p^5\,3d^2$	o	$^2P_{1/2}$	–	7238076	7235908	–
210	$2s^2\,2p^5\,3d^2$	o	$^2F_{7/2}$	**7236000?**	7241831	7242818	–
211	$2s^2\,2p^5\,3d^2$	o	$^2D_{5/2}$	**7240000?**	7251131	7246119	–
212	$2s^2\,2p^5\,3d^2$	o	$^2D_{3/2}$	–	7257952	7253388	–
213	$2s^2\,2p^5\,3d^2$	o	$^2P_{3/2}$	**7266000?**	7269242	7263947	–
214	$2s^2\,2p^5\,3d^2$	o	$^2P_{1/2}$	–	7309222	7303627	–
215	$2s\,2p^6\,3p^2$	e	$^4P_{1/2}$	–	7384058	7374540	–
216	$2s\,2p^6\,3p^2$	e	$^2D_{5/2}$	–	7389574	7381183	–
217	$2s\,2p^6\,3p^2$	e	$^2D_{3/2}$	–	7390566	7382311	–
218	$2s\,2p^6\,3p^2$	e	$^4P_{3/2}$	–	7395633	7386567	–
219	$2s\,2p^6\,3p^2$	e	$^4P_{5/2}$	–	7411114	7401807	–
220	$2s\,2p^6\,3p^2$	e	$^2P_{1/2}$	–	7418366	7408049	–
221	$2s\,2p^6\,3p^2$	e	$^2P_{3/2}$	–	7435885	7425663	–
222	$2s\,2p^6\,3s\,3d$	e	$^4D_{1/2}$	–	7480669	7473130	–
223	$2s\,2p^6\,3s\,3d$	e	$^4D_{3/2}$	–	7481725	7473674	–
224	$2s\,2p^6\,3s\,3d$	e	$^4D_{5/2}$	–	7483510	7474659	–
225	$2s\,2p^6\,3s\,3d$	e	$^4D_{7/2}$	–	7486075	7476203	–
226	$2s\,2p^6\,3p^2$	e	$^2S_{1/2}$	–	7506071	7491289	–
227	$2s\,2p^6\,3s\,3d$	e	$^2D_{3/2}$	–	7552884	7537978	–
228	$2s\,2p^6\,3s\,3d$	e	$^2D_{5/2}$	–	7556269	7540221	–
229	$2s\,2p^6\,3s\,3d$	e	$^2D_{3/2}$	–	7600455	7583866	–
230	$2s\,2p^6\,3s\,3d$	e	$^2D_{5/2}$	–	7600984	7583934	–
231	$2s^2\,2p^5\,3s\,4s$	o	$^4P_{5/2}$	–	7655895	7668872	–
232	$2s^2\,2p^5\,3s\,4s$	o	$^4P_{3/2}$	–	7667243	7679557	–
233	$2s^2\,2p^5\,3s\,4s$	o	$^2P_{1/2}$	–	7677217	7689062	–
234	$2s^2\,2p^5\,3s\,4s$	o	$^2P_{3/2}$	–	7691383	7701732	–
235	$2s\,2p^6\,3p\,3d$	o	$^4F_{3/2}$	–	7716155	7709523	–
236	$2s\,2p^6\,3p\,3d$	o	$^4F_{5/2}$	–	7721250	7713928	–
237	$2s\,2p^6\,3p\,3d$	o	$^4F_{7/2}$	–	7729551	7721465	–
238	$2s\,2p^6\,3p\,3d$	o	$^4F_{9/2}$	–	7740363	7731661	–
239	$2s\,2p^6\,3p\,3d$	o	$^2D_{5/2}$	–	7749958	7740486	–
240	$2s\,2p^6\,3p\,3d$	o	$^2D_{3/2}$	–	7753184	7743954	–

This paper has been typeset from a TEX/LATEX file prepared by the author.